Gene expression changes controlling distinct adaptations in the heart and skeletal muscle of a hibernating mammal

Katie L. Vermillion, Kyle J. Anderson, Marshall Hampton and Matthew T. Andrews

---

You might find this additional info useful...

Supplemental material for this article can be found at:
/content/suppl/2015/01/15/physiolgenomics.00108.2014.DC1.html

This article cites 107 articles, 45 of which can be accessed free at:
/content/47/3/58.full.html#ref-list-1

Updated information and services including high resolution figures, can be found at:
/content/47/3/58.full.html

Additional material and information about *Physiological Genomics* can be found at:
http://www.the-aps.org/publications/pg

This information is current as of March 1, 2015.

Gene expression changes controlling distinct adaptations in the heart and skeletal muscle of a hibernating mammal

Katie L. Vermillion,[1] Kyle J. Anderson,[1] Marshall Hampton,[2] and Matthew T. Andrews[1]

[1]*Department of Biology, University of Minnesota Duluth, Duluth, Minnesota; and* [2]*Department of Mathematics and Statistics, University of Minnesota Duluth, Duluth, Minnesota*

Vermillion KL, Anderson KJ, Hampton M, Andrews MT. Gene expression changes controlling distinct adaptations in the heart and skeletal muscle of a hibernating mammal. *Physiol Genomics* 47: 58–74, 2015. First published January 8, 2015; doi:10.1152/physiolgenomics.00108.2014.—Throughout the hibernation season, the thirteen-lined ground squirrel (*Ictidomys tridecemlineatus*) experiences extreme fluctuations in heart rate, metabolism, oxygen consumption, and body temperature, along with prolonged fasting and immobility. These conditions necessitate different functional requirements for the heart, which maintains contractile function throughout hibernation, and the skeletal muscle, which remains largely inactive. The adaptations used to maintain these contractile organs under such variable conditions serves as a natural model to study a variety of medically relevant conditions including heart failure and disuse atrophy. To better understand how two different muscle tissues maintain function throughout the extreme fluctuations of hibernation we performed Illumina HiSeq 2000 sequencing of cDNAs to compare the transcriptome of heart and skeletal muscle across the circannual cycle. This analysis resulted in the identification of 1,076 and 1,466 differentially expressed genes in heart and skeletal muscle, respectively. In both heart and skeletal muscle we identified a distinct cold-tolerant mechanism utilizing peroxisomal metabolism to make use of elevated levels of unsaturated depot fats. The skeletal muscle transcriptome also shows an early increase in oxidative capacity necessary for the altered fuel utilization and increased oxygen demand of shivering. Expression of the fetal gene expression profile is used to maintain cardiac tissue, either through increasing myocyte size or proliferation of resident cardiomyocytes, while skeletal muscle function and mass are protected through transcriptional regulation of pathways involved in protein turnover. This study provides insight into how two functionally distinct muscles maintain function under the extreme conditions of mammalian hibernation.

hibernation; transcriptomics; heart; skeletal muscle

HIBERNATION IS AN ADAPTIVE phenotype used by many mammalian species to survive predictable periods of low nutrient availability. Most hibernators cycle between long bouts of torpor (TOR) that are interrupted by brief interbout arousals (IBAs) throughout hibernation. When thirteen-lined ground squirrels (*Ictidomys tridecemlineatus*) enter TOR they decrease their heart rate from 300–400 bpm to 3–10 bpm, reduce their body temperature (T_b) as low as 2–10°C, and exhibit reduced oxygen consumption and basal metabolic rate for 7–10 days (5, 20). During IBAs they quickly rewarm over 2–3 h and return to a normothermic physiological state, before returning to torpor 12–24 h later (5). These extreme changes occur in only a few hours as the animals quickly warm themselves for an IBA or cool down while entering TOR. These physiological

extremes and the quick transitions between them pose major challenges to the physiology of a hibernating mammal.

Skeletal and cardiac muscle are two contractile tissues that experience very different functional demands during hibernation. The heart must maintain function throughout a wide range of temperatures and metabolic conditions (52). Skeletal muscle remains largely immobile for 5–6 mo yet must resume full functionality during the IBAs and upon waking in the final arousal in spring if the animal is to forage and evade predation. The adaptations that these organisms use to maintain their tissues under such variable conditions serve as a natural model to study a variety of medically relevant conditions including heart failure and muscle disuse atrophy.

Conditions experienced by the heart during hibernation such as rapid temperature changes and fluctuations in oxygen and nutrient levels would result in ventricular fibrillation (VF) or severe arrhythmias in humans (93). Hibernators hearts are resistant to VF, and several mechanisms are thought to contribute to maintaining normal cardiac function at reduced temperatures and metabolic states (53). The hearts of mammalian hibernators exhibit a different adrenergic innervation of the ventricle, which is thought to offer a protective mechanism against VF at low temperatures (71). Additionally, enhanced calcium handling in the heart provides a more efficient way to clear cytosolic calcium stores and thus preventing calcium overload, which occurs in nonhibernators at reduced temperatures (10, 17, 63, 103, 107). Others attribute the cold resistance to the hibernator's ability to decrease saturation of depot fats, making these lipids available for fuel utilization throughout the hibernation season (28). Moreover, optimal cardiac function is thought to be maintained by increased rates and efficiency of energy production and utilization in the cardiac tissue, including altered enzyme functionality and alternate metabolic pathway utilization (13, 54).

Hibernation also presents unique challenges to skeletal muscle, in that it is a highly abundant and metabolically expensive tissue that is under strong selective pressure to maintain functionality despite its disuse during hibernation. The degree of inactivity experienced by skeletal muscle during TOR would lead to disuse atrophy and an associated slow-to-fast shift in muscle fiber type in nonhibernators (78, 91). Hibernator skeletal muscle exhibits protection from disuse atrophy and shifts to a slow muscle fiber type in preparation for the hibernation season (4, 73). Slow muscle has higher oxidative potential and low fatigability, making it ideal for utilizing fatty acids as an energy source and for performing the extended periods of shivering thermogenesis essential to the rewarming process (86). Postulated mechanisms of atrophy avoidance include depressed levels of protein degradation and periodic bursts of protein synthesis associated with arousals (58). This proposed

mechanism would reduce the metabolic demand of skeletal muscle by inhibiting protein turnover for the majority of the hibernation season (105).

To make an in-depth comparison between these two striated muscle types that serve functionally distinct roles throughout hibernation, we used Illumina high-throughput sequencing technology to analyze mRNA levels in cardiac and skeletal muscle tissues across the circannual cycle. Although the majority of genes expressed in these two tissue types are the same, their differential expression throughout the circannual cycle more clearly defines the molecular mechanisms and pathways used by these two similar muscle tissues that allow them to serve very diverse functions during hibernation. Cardiac tissue relies on diverse fuel sources to maintain tissue integrity and contractility throughout the hibernation season, as well as expression of the fetal cardiac gene expression profile for cardioprotection, whereas skeletal muscle relies on muscle fiber type switching and unique control of protein turnover to maintain functionality and tonality.

MATERIALS AND METHODS

Animals

Thirteen-lined ground squirrels, *I. tridecemlineatus*, were live-trapped near Paynesville, MN, and housed in the Association for Assessment and Accreditation of Laboratory Animal Care-accredited Animal Care Facility at the University of Minnesota Duluth School of Medicine. Squirrels are individually housed in plastic top-load rat cages with aspen shavings. The squirrels were housed under standard conditions in a 12:12 light/dark cycle at 23°C and fed standard rodent chow and water ad libitum from April to October. During the hibernation season (November-March), the squirrels were moved into an artificial hibernation chamber and kept in constant darkness at 5–7°C with no food provided and water ad libitum. All experimental animal procedures were approved by the University of Minnesota Institutional Animal Care and Use Committee (protocol #1103A97712).

Experimental Collection Points

Four collection points were chosen for these experiments to reveal the most meaningful comparisons in ground squirrel heart and skeletal muscle tissues across the hibernation season. The four collection points used were: prehibernation [October active (OCT)], TOR, IBA, and posthibernation [April active (APR)]. Three males and three females were killed at each collection point. Animal state at each collection point was determined by rectal temperature and animal behavior. All animals were collected between 10 AM and 3 PM.

For the October collection point the animals have increased body mass in the preceding months and are preparing for hibernation. October animals are experiencing shallow TOR bouts, in which T_b drops as low as 20°C for up to 24 h. This time point represents an opportunity to detect transcriptional changes associated with preparation for hibernation. All animals collected at this time point were held at 12:12 light/dark cycle at 23°C and had water and food ad libitum. October active animals were collected in the first 2 wk of October and were active at the time of death, with a T_b of 35–37°C and were observed as awake and active (open eyes and coordinated body movements).

The TOR and IBA collection points reflect the extreme conditions that hibernating ground squirrels experience. During TOR ground squirrels drop their T_b, reduce oxygen consumption, and dramatically reduce their heart rates (65). Throughout hibernation ground squirrels experience IBAs, in which T_b, heart rate, and oxygen consumption return to normal rates. This process occurs on average every 7–10 days, and the return to normothermic conditions occurs over the course of 2–3 h, at which time animals are awake and active for 12–24

h and exhibit coordinated body movements. These collection points are important in showing the changes that orchestrate these drastic physiological changes. The sawdusting method was used to identify the squirrels in TOR and IBA. Animals in TOR were collected after a minimum of 3 days in a TOR bout and showed no visible signs of arousal. At the time of death rectal temperatures was taken to verify torpid state (T_b 6–8°C). Animals collected for the IBA collection point aroused naturally and were awake and active and showed coordinated body movement. Rectal temperatures collected at death showed an active T_b between 35 and 37°C. TOR and IBA animals were collected in January and February, when TOR bouts are the longest.

The April collection point reflects the posthibernation state of the animal, when the animal is recovering from the hibernation season, resuming food consumption, and preparing for reproduction. These animals were removed from the hibernation chambers at the end of March and returned to a 12:12 light/dark cycle at 23°C with food and water ad libitum. The animals for the April collection point were collected in the second and third weeks of April.

Heart Dissection

All animals were fully anesthetized with isoflurane and then killed by decapitation. The pericardium was removed from around the heart, the heart was removed from the animal and halved sagitally to include both atria and ventricle. Heart dissection was performed on ice and dissected heart pieces were rapidly flash-frozen in liquid nitrogen. The two sagittal halves were frozen and stored separately. The time from decapitation to sample freezing was <10 min. Tissues were stored at −80°C until RNA purification.

Skeletal Muscle Dissection

All animals were fully anesthetized with isoflurane and then killed by decapitation. The quadriceps femoralis was removed from the upper thigh, further dissected into smaller pieces, and rapidly flash-frozen in liquid nitrogen. The two quadriceps femoralis muscles were frozen and stored separately. The time from decapitation to sample freezing was < 10 min. Tissues were stored at −80°C until RNA purification.

RNA Preparation

RNA was purified from heart and skeletal muscle samples using a Qiagen RNeasy Mini Kit, and remaining genomic DNA was removed using an Ambion DNase kit. One sagittal half of the heart from each animal was used for RNA purification. The quadriceps femoralis from each animal was used for RNA purification. For RNA quality control, the protein concentration was determined using a Nanodrop and then 1 μg of each sample was run on an agarose gel to look for distinct 28s and 18s bands. RNA from one male and one female from each collection point was combined together in a single sample, and each collection point contained three pooled samples. Samples were pooled to eliminate variation due to sex. Samples were sent to the University of Minnesota Biomedical Genomics Center (Minneapolis, MN) for Illumina HiSeq 2000 Sequencing.

Sample Quality Assessment

Total RNA isolates were quantified with a fluorimetric RiboGreen assay. Total RNA integrity was assessed by capillary electrophoresis and generated an RNA integrity number (RIN). All of the samples passed the initial quality control step verifying them as high quality samples (>1 μg, RIN = 8+). RNA samples were converted to Illumina sequencing libraries using Illumina's Truseq RNA Sample Preparation Kit (RS-122-2001).

Library Creation

From each heart and skeletal muscle replicate 1 μg of total RNA (equal RNA from male and female) was enriched for mRNA using

oligo-dT-coated magnetic beads, fragmented, and reverse-transcribed into cDNA. The cDNA was fragmented, blunt-ended, and ligated to indexed (barcoded) adaptors and amplified using 15 cycles of PCR. Final library size distribution was validated by capillary electrophoresis and quantified with PicoGreen fluorimetry and qPCR. Libraries were successfully sequenced for all samples.

Cluster Generation and Sequencing

Truseq libraries were hybridized to a paired-end flow cell, and individual fragments were clonally amplified by bridge amplification on the Illumina cBot. Libraries were clustered at a concentration of 12 pM. After clustering the flow cell was loaded on the HiSeq 2000 and sequenced using Illumina's Sequencing by Synthesis chemistry. Upon completion of a read, a 7-base pair index read is performed. Samples were run for 100 cycles with a minimum of 10 million single reads per sample. Base call (.bcl) files for each cycle of sequencing were generated by Illumina Real Time Analysis software. The base call files and run folders were then exported to servers maintained at the Minnesota Supercomputing Institute (Minneapolis, MN). Primary analysis and demultiplexing were performed with Illumina's CASAVA software 1.8.2, resulting in demultiplexed FASTQ files.

Bioinformatics Analysis

Over 10 million raw sequence reads were generated per sample. These reads were mapped to a set of *I. tridecemlineatus* contigs assembled in the open-source program Trinity (35). The contigs were constructed from consensus regions of DNA from these data in addition to previous *I. tridecemlineatus* RNA-seq experimental data from brain cortex, hypothalamus (88), brown adipose tissue (BAT) (37), and white adipose tissue (WAT). Trinity was used to predict coding domain subsequences within these contigs to specifically select for protein-coding transcripts. Any contig containing a predicted coding domain was selected and trimmed to include only this domain plus up to 100 bases on both ends of the domain. Before reads were matched to the contigs, mitochondrially encoded genes were screened out by the use of the thirteen-lined ground squirrel mitochondrial genome sequence (38) and the National Center for Biotechnology Information's (NCBI's) megablast program (2) because of the high density of mitochondrial genomes in heart and skeletal muscle. The selected contigs were then compared with the NCBI RefSeq human mRNA sequences using NCBI Blastn (2). Raw reads from each experimental sample were identified using these contigs and then quantified using the counts for each gene. Gene names used for identification are the official Human Genome Organisation Gene Nomenclature Committee designations.

Resulting read counts were normalized to the upper quartile and then fitted to a negative binomial distribution using DESeq v1.6.1 (3). All genes included in the initial analysis of heart and skeletal muscle had at least 10 read counts total across the four time points. All read counts across all collection points were quantified for each mRNA to determine overall abundance for heart and skeletal muscle. Maximum fold change for each gene was calculated as the collection point with the highest average read counts by the collection point with the lowest average read counts. Tissue specificity for heart and skeletal muscle was calculated for each gene by dividing the percentage of read counts in that tissue divided by the total number of read counts in all other transcriptomic samples, including heart, skeletal muscle, along with cortex, hypothalamus (88), BAT (37), and WAT (38), which were obtained from other transcriptomic experiments.

Differential Gene Expression

Differential gene expression was determined for heart and skeletal muscle using an analysis of deviance in DESeq v1.6.1, to generate a test statistic (*P* value) using the methods described by Anders and Huber (3). Each collection point consisted of three pooled samples

from both heart and skeletal muscle. We independently filtered the computed *P* values (16) by restricting those with at least a 50% change between any two collection points and at least one collection point with a mean of 100 or more reads. The Benjamini-Hochberg method was then used to correct for multiple comparisons, providing a *P* value cutoff for significance, which controlled the false discovery rate (FDR) at 0.05. For heart and skeletal muscle, any transcript with a *P* value less than the respective cutoff value was considered differentially expressed (FDR < 0.05). All differentially expressed genes for heart and skeletal muscle are listed in Supplemental Table S1, along with their means, standard errors, fold changes (in relation to the April collection point), and *P* values.[1] On these differentially expressed genes (heart = 1,076; skeletal muscle = 1,466), post hoc pair-wise comparisons were performed using the same function in DESeq v1.6.1, but with different input data. For this pair-wise analysis, the *P* values were independently filtered (16) to restrict to a 50% change between two specific collection points, rather than any two. The Benjamini-Hochberg method was used to control the FDR to 0.05 to correct for multiple comparisons. Pair-wise comparisons are listed in Supplemental Table S2.

Functional Annotation Clustering

The differentially expressed transcripts from heart and skeletal muscle were analyzed with the functional annotation tools of DAVID (45) and literature searches. Genes were first sorted for differential expression relative to APR and then sorted for genes that were upregulated and downregulated. These lists were entered into DAVID separately for analysis. DAVID analysis provided annotation and gene GO-term enrichment analysis. DAVID functional annotation clustering (FAC) was used for further analysis (46). DAVID FAC uses an algorithm to measure the relationships among the annotation terms. Each annotation term inside each cluster is assigned a *P* value (Fisher exact/EASE score), and these *P* values are used to calculate a group enrichment score. This score is the geometric mean of the member's *P* values in a corresponding annotation cluster and is used to rank their biological significance. The number of genes involved in the term is also given in Table 3.

RESULTS

Overview

The goal of this study was to use advanced high-throughput sequencing technologies to compare gene expression between the heart and skeletal muscle of the thirteen-lined ground squirrel throughout the hibernation season. Total RNA was prepared from heart and skeletal muscle at four time points throughout the circannual cycle: APR, OCT, TOR, and IBA (Fig. 1). Illumina HiSeq 2000 sequencing of cDNAs derived from 24 animals resulted in 88,878,967 high-quality reads of 100 bases each for heart and 109,274,656 for skeletal muscle (Table 1). Contig assembly resulted in the identification of 14,332 distinct transcripts in ground squirrel heart and 14,169 transcripts in skeletal muscle. Only transcripts that had 10 reads at any time point were used for further analysis. This resulted in 8,285 protein-coding genes in heart and 8,278 genes in skeletal muscle, with 8,229 being expressed in both tissues. The fact that 99% of the genes are expressed in both heart and skeletal muscle highlights the homology between these two tissues.

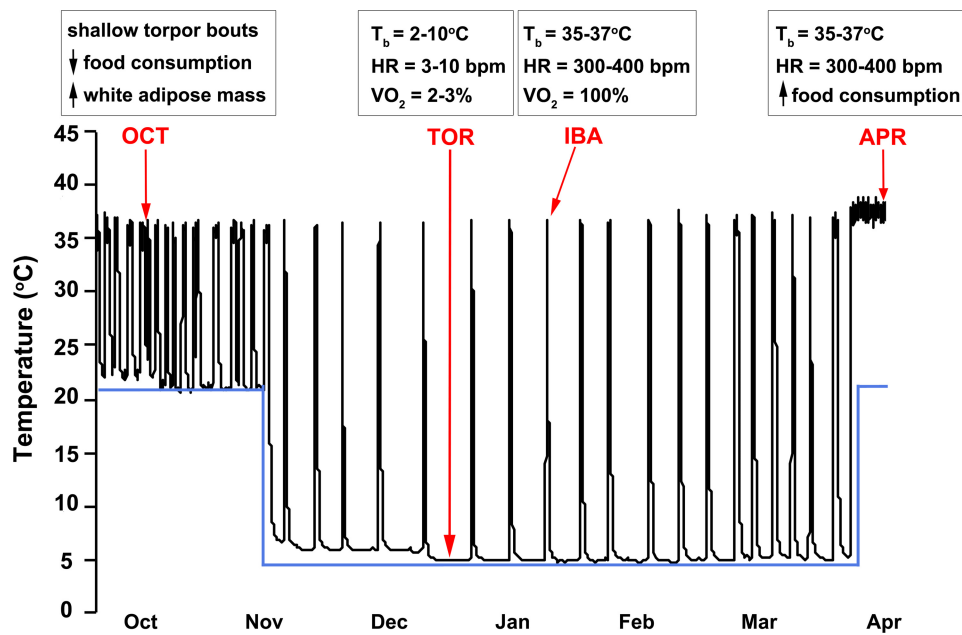[1] The online version of this article contains supplemental material.

Fig. 1. Body temperature (T_b) recordings and physiological characteristics across the hibernation season. Core T_b (black line) from a single animal measured by a surgically implanted transmitter, along with the controlled ambient temperature (blue line) of the environmental chamber over the course of the hibernation season. Red arrows indicate representative T_b at each of the time points collected: OCT (October), TOR (torpor), IBA (interbout arousal), and APR (April). A brief description of the physiological and behavioral characteristics at each of the time points is provided in the boxes above each time point.

Tissue Specificity

Despite 99% of the genes being expressed in both tissues, the heart and skeletal muscle show different levels of tissue specificity. Figure 2 shows the number of transcripts that were identified with >75% specificity for each tissue type, relative to the other five ground squirrel tissues on which we have previously performed transcriptome analysis (brown and white adipose, hypothalamus, cortex, heart, and skeletal muscle) (37, 38, 88). Of those transcripts, the skeletal muscle has twice as many mRNAs with >95% specificity compared with the heart. However, only one transcript, immunoglobulin-like and fibronectin type III domain containing 1 (*IGFN1*) (Fig. 2*B*), is 100% specific for skeletal muscle, while four transcripts are 100% specific for heart, including the cardiac transcription factors *NKX2.5* and *TBX20* (Fig. 2*A*).

Ranked Abundance

There are many functional similarities between the most highly expressed genes in heart and skeletal muscle. Figure 3 shows the 20 most abundant transcripts in heart (Fig. 3*A*) and skeletal muscle (Fig. 3*B*). Of these 20 transcripts, only four are expressed in both tissues. Tropomyosin-1 (*TPM-1*), titin (*TTN*), and glyceraldehyde 3-phosphate dehydrogenase (*GAPDH*) are more

Table 1. *Overview of Illumina HiSeq2000 RNAseq data*

	Heart	Skeletal
High-quality reads	88,878,967	109,274,656
Distinct transcripts	14,332	14,169
Protein-coding genes	8,285	8,278
Genes expressed in both	8,229	
Differentially expressed genes	1,076	1,466
Genes differentially expressed in both	369	

Samples were run for 100 cycles with a minimum of 10 million single reads per sample. Contig assembly and prediction of protein-coding domains were performed in Trinity. All identified genes have at least 10 counts at any one time point. Differentially expressed genes show at least a 50% change between 2 collection points and have a false discovery rate (FDR) < 0.05.

abundant in skeletal muscle, while myoglobin (*MB*) is more abundant in the heart. Although there are only four transcripts that are expressed in both tissues, several tissue specific isoforms of various proteins are expressed and are among the most abundant transcripts for both heart and skeletal muscle. The most abundant transcripts in both tissues are various forms of myosin heavy chain (MYH), with the cardiac isoforms of *MYH6* and *MYH7* and the skeletal muscle isoforms *MYH1*, *MYH2*, and *MYH4* being among the 20 most abundant transcripts in the heart and skeletal muscle, respectively. Additionally, several isoforms of myosin light chain (MYL) are among the most abundant transcripts in both heart (*MYL2*, *MYL3*) and skeletal muscle (*MYL1*, *MYLPF*). Other examples of tissue-specific isoform expression come from additional factors important for regulating muscle contraction, including the sarco/endoplasmic reticulum Ca^{2+}-ATPase (ATP2A) with *ATP2A1* being the predominant form in fast-twitch skeletal muscle and *ATP2A2* in the heart. Troponin (TNN), which is essential for regulating muscle contraction in both cardiac and skeletal muscle, has the cardiac-specific isoform *TNNT2* in the heart and *TNNT3* and *TNNI2* in skeletal muscle, ranking among the 20 most abundant transcripts.

Only small subsets of the 20 most abundant transcripts are differentially expressed (FDR < 0.05) over the four collection points (Supplemental Table S1). *MYH6* is the only transcript that is differentially expressed in the heart showing the highest expression in TOR, while *MYH2*, *MYH4*, *MB*, and actinin alpha 2 (*ACTN2*) are differentially expressed in the skeletal muscle, with *MYH2*, *MYH4*, and *ACTN2* showing highest expression in APR, while *MB* expression peaks in OCT.
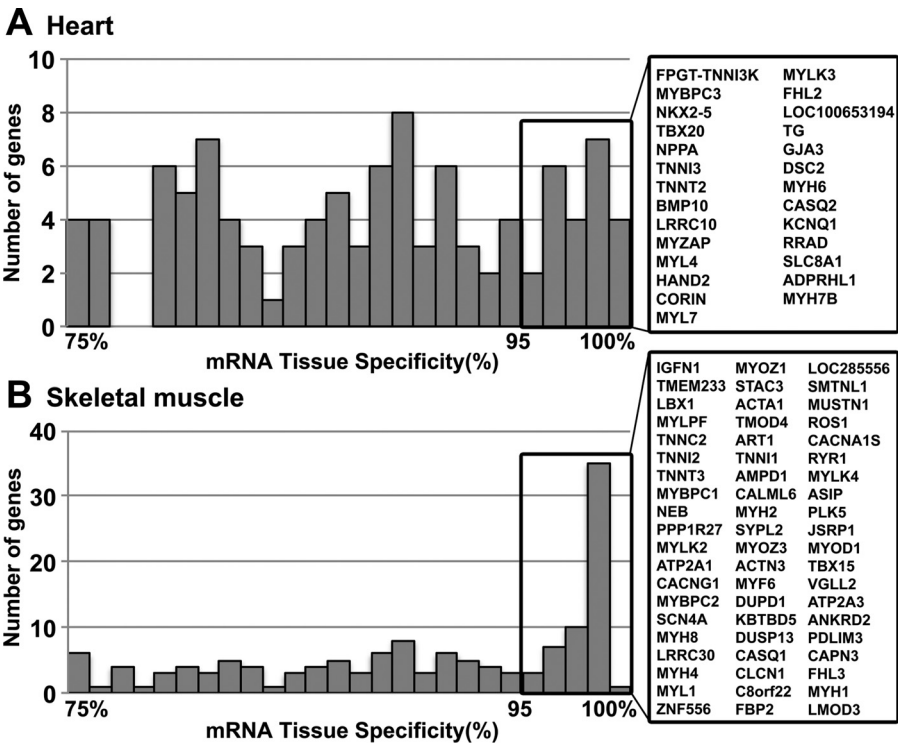
Differential Expression

We determined differential expression across the four collection points by independently filtering *P* values computed by DESeq. Genes are considered differentially expressed if they have at least 100 normalized counts in one collection point and have at least a 50% change between the means of any two

A Heart

Fig. 2. Heart and skeletal muscle tissue specificity. The graph represents the number of genes that show 75–100% expression specific for heart (*A*) and skeletal muscle (*B*) relative to the 6 tissues transcriptome analysis has been performed on (see MATERIALS AND METHODS). A value of 100% specificity means that gene is expressed only in that tissue. Genes showing 95% or greater specificity are listed in the box to the *right* of each graph, in descending order of specificity. Genes are listed by Human Genome Organisation Gene Nomenclature Committee (HGNC) designations.

Heart gene box:
FPGT-TNNI3K	MYLK3
MYBPC3	FHL2
NKX2-5	LOC100653194
TBX20	TG
NPPA	GJA3
TNNI3	DSC2
TNNT2	MYH6
BMP10	CASQ2
LRRC10	KCNQ1
MYZAP	RRAD
MYL4	SLC8A1
HAND2	ADPRHL1
CORIN	MYH7B
MYL7	

B Skeletal muscle

Skeletal muscle gene box:
IGFN1	MYOZ1	LOC285556
TMEM233	STAC3	SMTNL1
LBX1	ACTA1	MUSTN1
MYLPF	TMOD4	ROS1
TNNC2	ART1	CACNA1S
TNNI2	TNNI1	RYR1
TNNT3	AMPD1	MYLK4
MYBPC1	CALML6	ASIP
NEB	MYH2	PLK5
PPP1R27	SYPL2	JSRP1
MYLK2	MYOZ3	MYOD1
ATP2A1	ACTN3	TBX15
CACNG1	MYF6	VGLL2
MYBPC2	DUPD1	ATP2A3
SCN4A	KBTBD5	ANKRD2
MYH8	DUSP13	PDLIM3
LRRC30	CASQ1	CAPN3
MYH4	CLCN1	FHL3
MYL1	C8orf22	MYH1
ZNF556	FBP2	LMOD3

collection points. Of the transcripts identified 1,076 genes were differentially expressed in heart, and 1,466 were differentially expressed in skeletal muscle, with only 369 being differentially expressed in both tissues. The expression patterns of the five genes showing the greatest fold change across collection points for both heart and skeletal muscle are presented in Fig. 4. Of the top five differentially expressed genes only *CYP1A1* is differentially expressed in both heart and skeletal muscle. *CYP1A1* is a member of the cytochrome P450 family, is a monooxygenase involved in the metabolism of xenobiotics (21), and is induced under hypoxic conditions (22, 75). *CYP1A1* shows the greatest fold change (60.5-fold) in the heart and the fifth highest fold change (33.9-fold) in skeletal muscle (Fig. 4, *A* and *J*). In skeletal muscle *CA1*, carbonic anhydrase 1, an enzyme that removes carbon dioxide from tissues by conversion to bicarbonate and protons (18), shows the greatest fold change (138-fold) (Fig. 4*F*). Decreased expression of these two genes in TOR correlates with reduced oxygen consumption during the decreased metabolic state. All 10 of the genes represented show the greatest reduction in expression during TOR and IBA. Of all differentially expressed genes, <3% showed a fivefold or greater change in expression, and only four of those genes are shared between heart and skeletal muscle: *CYP1A1*, *DDIT4*, *ADAMTS1*, and *PM20D2* (Supplemental Table S1). All four genes show peak expression in APR in the heart; however, *CYP1A1* shows peak expression in OCT in skeletal muscle. *PM20D2* is involved in metabolite repair (100), which may be required to repair metabolites damaged throughout the hibernation season. Post hoc pair-wise comparisons between any two collection points showed that the highest number of statistically significant changes occurred between TOR and APR, in both heart and skeletal muscle (Table 2; italics, Supplemental Table S2). Interestingly, the two time points showing the fewest statistically significant

changes in both heart and skeletal muscle are between the two hibernation points TOR and IBA.

Functional Analysis

Fuel utilization. Differentially expressed genes were functionally clustered using the Database for Annotation, Visualization and Integrated Discovery (DAVID) to highlight functional pathways that are altered across the circannual cycle of a hibernator. Genes were first sorted by their expression relative to April and then further sorted into genes that were upregulated or downregulated. The top five FACs are shown for each time point for heart and skeletal muscle in Table 3. In both the heart and skeletal muscle there is evidence that mitochondrial function, including fatty acid metabolism, is especially important for the hibernation phenotype. Transcripts associated with fatty acid metabolism are upregulated in OCT, TOR, and IBA in both heart and skeletal muscle (Fig. 5*A*). In support of previous findings that fatty acids are the primary fuel source during hibernation, we see increased expression of many of the key players utilized during fatty acid metabolism including *FABP3*, *ACOT1*, *ACSL1*, *ACSL3*, *ACSL4*, and *ACSL6*. These genes encode important enzymes in the conversion of free long-chain fatty acids into fatty-acyl CoA. Fatty acids are transported across the mitochondrial membrane by *CPT1A*, *CPT1B*, and *SLC25A20*, all of which are significantly increased in heart and/or skeletal muscle during hibernation. Additionally, the enzymes required for β-oxidation of fatty-acyl CoA are significantly upregulated, including *ACADS*, *ACADVL*, *ACAD10*, *ECH1*, *ACOT2*, *HADHA*, and *HADHB* in heart and/or skeletal muscle. Catalase (*CAT*) and peroxiredoxin (*PRDX5*) are responsible for the breakdown of hydrogen peroxide produced in β-oxidation, and both are upregulated in skeletal muscle beginning in OCT or throughout hibernation.

A Ranked Abundance: Heart
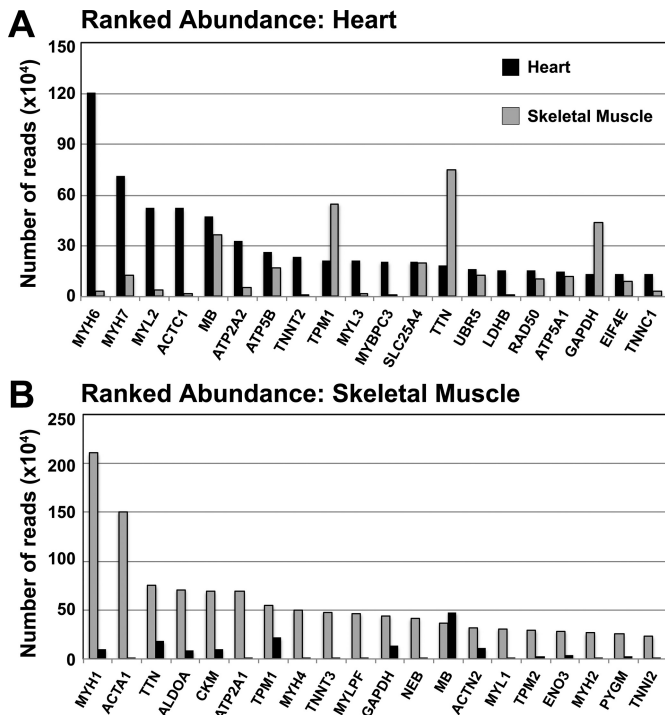

B Ranked Abundance: Skeletal Muscle

Fig. 3. Most abundant transcripts in heart and skeletal muscle. The total number of reads across all collection points for each mRNA were used to determine overall abundance for heart and skeletal muscle. The 20 most abundant transcripts are represented for heart (*A*) and skeletal muscle (*B*), with the corresponding counts for the other tissue also represented in each graph for comparison. Heart mRNA abundance is represented in black; skeletal muscle mRNA is represented in gray. Transcripts are listed by HGNC designations.

Enzymes involved in the degradation of branched chain fatty acids are significantly downregulated, for example, *ACADSB*. This is consistent with previous findings of reduced expression of proteins associated with mitochondrial β-oxidation of branched chain fatty acids (34).

Upregulation of peroxisomal fatty acid metabolism. The deep sequencing methods used in this study made it possible for us to identify an additional metabolic pathway not previously reported as being differentially regulated during hibernation either in the heart or skeletal muscle. In addition to mitochondrial fatty acid metabolism there is increased expression of genes involved in peroxisomal fatty acid metabolism, which is important for breaking down very long chain and unsaturated fatty acids, making them more accessible for mitochondrial β-oxidation. Peroxisomal metabolism is significantly enriched in the heart in OCT, TOR, and IBA (Table 3) and shows similar regulation in skeletal muscle. Several of the transcripts for key enzymes in the peroxisomal β-oxidation pathway are upregulated in TOR relative to APR, including the multifunctional enzyme *HSD17B4* and the thiolase *ACAA1*, which are required for the degradation of straight-chain saturated fatty acids (Fig. 5*B*). The peroxisome-specific thioesterase, *ACOT4*, also shows increased expression during TOR. Additionally, several auxiliary enzymes, which are required for the β-oxidation of unsaturated fatty acids, are increased including *DECR2* and *ECH1*. This correlates with increased unsaturated fatty acids found in fat depots in thirteen-lined ground squirrels (28). In addition to increased β-oxidation of fatty acids in the peroxisome during hibernation, we also see in-

creased expression of genes associated with α-oxidation of fatty acids, including the lyase HACL1. Several other peroxisomal proteins were significantly upregulated in TOR and IBA in the heart and/or skeletal muscle including *HSDL2*, *MVD*, *EPHX2*, and the peroxisomal biogenesis factor *PEX19*.

Even though fatty acid metabolism serves as the primary fuel source during hibernation for both heart and skeletal muscle, we see a divergent pattern of expression in genes associated with glycolysis between the two tissues. Our data show a trend toward increased expression in almost all of the enzymes of the glycolytic pathway in the heart in TOR relative to APR or OCT; however, only a few show statistically significant increases, including *GCK, HK1, PFKM,* and *PGAM2* (Fig. 6). In skeletal muscle we see a trend toward decreased expression in almost all of the glycolytic enzymes in TOR relative to APR, with *GCK, HK2,* and *ENO1* showing significantly decreased expression. Although both muscle types show similar mechanisms of utilizing fuel during the extremely dynamic metabolic shifts associated with hibernation, this finding highlights a key difference in the energetic demands of heart and skeletal muscle during the hibernation season.

Increased oxidative capacity of skeletal muscle. Following increased β-oxidation in the mitochondria and peroxisomes, we see increases in TCA cycle enzymes in skeletal muscle, including isocitrate dehydrogenase 3 (IDH3A) and aconitase (ACO2) (Fig. 7). Without seeing a clear increase in genes directly associated with oxidative phosphorylation, we see skeletal muscle-specific increases in genes involved in iron-protein assembly and oxygen transport. Angiogenic growth factors *VEGFA* and *VEGFB* show peak expression in OCT and elevated expression in hibernation in skeletal muscle (Fig. 7), while *ADAMTS1*, a protein with antiangiogenic activity (64, 99), shows significantly decreased expression in TOR (Supplemental Table S1). Iron uptake, heme, and MB synthesis begin in OCT with a spike in gene expression of transferrin receptor (*TFRC*), the rate-limiting enzyme in heme synthesis *ALAS1*, and *MB* along with reduced expression of heme degradative enzymes *HMOX1, HMOX2,* and *POR* in skeletal muscle. The iron-sulfur cluster assembly enzyme (*ISCU*), mitochondrial iron transporter *SLC25A28*, the mitochondrial heme transporter *ABCB6*, the electron transfer flavoprotein-ubiquinone oxidoreductase (*ETFDH*), and the cytochrome c oxidase subunit *COX7A2L* are all upregulated in skeletal muscle during the hibernation season and are all involved in the production of heme and iron-related proteins. Expression of the transcriptional coactivator implicit in a variety of mitochondrial functions, PPAR-γ coactivator-1alpha (*PPARGC1A*) peaks in OCT and returns to APR levels in TOR and IBA in skeletal muscle. In both heart and skeletal muscle the homolog PGC-1β (*PPARGC1B*) is expressed at peak levels during TOR and IBA. Each of these transcriptional coactivators have been shown to promote expression of genes associated with increased oxidative capacity, as seen above. This increase in oxidative capacity is much more pronounced in the skeletal muscle, likely because of the inherently high oxidative capacity of the heart (32).

Tissue-specific Muscle Maintenance

Cardiac and skeletal muscles differentiate early in vertebrate embryogenesis and require the combinatorial actions of multiple signaling pathways (81). The mechanisms of maintaining
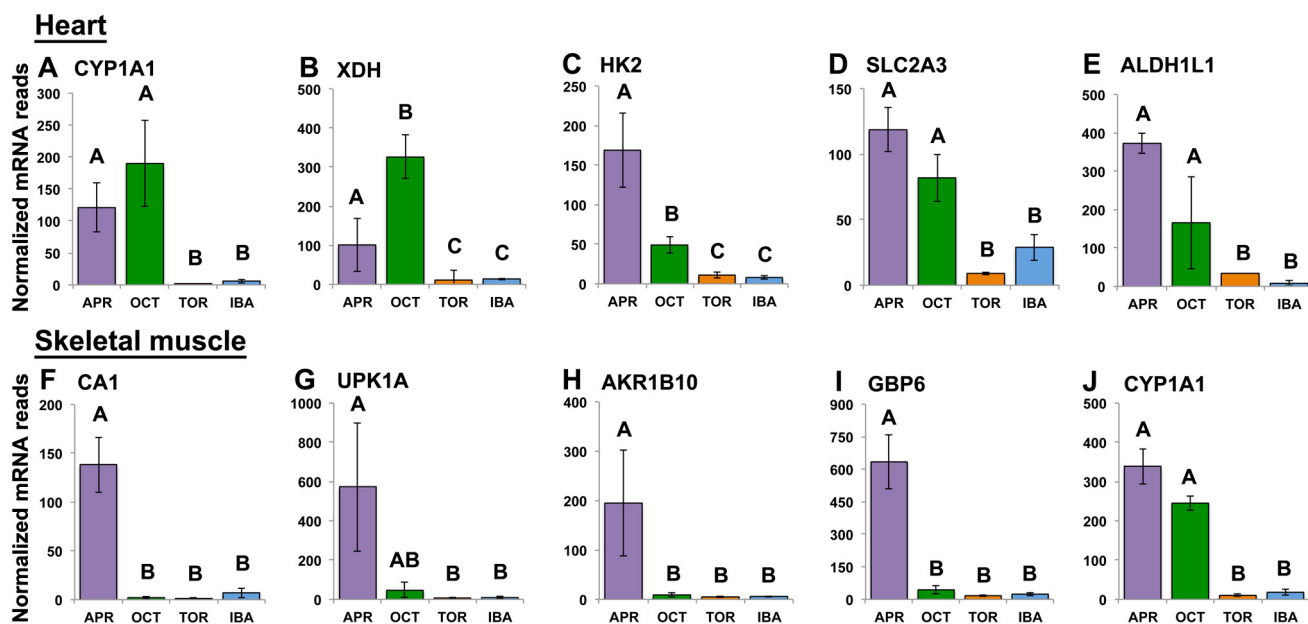
Fig. 4. Genes showing the greatest fold change for heart and skeletal muscle across the circannual cycle. Greatest fold change for each gene was calculated by dividing the collection point with the highest average read counts by the collection point with the lowest average read counts for heart (*A–E*) and skeletal muscle (*F–J*). Within each tissue genes are listed in descending order of greatest fold change. All genes represented are differentially expressed with a false discovery rate (FDR) < 0.05. Error bars represent the SE. Post hoc pair-wise comparisons were used to determine differential expression between any 2 time points. Any time point not sharing the same letter is significantly different (FDR < 0.05). Genes are listed by HGNC designations.

and remodeling cardiac and skeletal muscle are of particular interest since both muscle types are capable of adapting to changing physiological and environmental conditions such as hibernation (9). Hypertrophy of both muscle types results from physical or pathological stress, while atrophy of skeletal muscle results from lack of physical activity. Evidence of the combinatorial and multifaceted signaling pathways used to maintain muscle integrity is evident in the transcriptome during hibernation.

Regulation of protein turnover. Transcriptomic analysis of skeletal muscle reveals several mechanisms by which hibernating mammals might avoid disuse atrophy, showing widespread differential expression of genes involved in protein synthesis and degradation. Genes involved in protein synthesis, including the mTOR pathway, show increased expression in skeletal muscle during the hibernation season. The key en-

zymes in this pathway that are upregulated are *AKT1*, *MTOR*, and *RPS6KB1* (Fig. 8*A*). Similarly, inhibitors of protein synthesis, *DDIT4*, *KLF15*, and *EIF4EBP1*, show decreased expression at the same time points. This pathway is likely regulated through IGF signaling in skeletal muscle during hibernation, with *IGF1* and *IGF2* showing significant upregulation in skeletal muscle, while the inhibitory IGF binding proteins *IGFBP2* and *IGFBP7* are significantly downregulated. We also see evidence of reduced protein degradation during the hibernation season, including reduced expression of the negative regulator of muscle growth myostatin (*MSTN*), the transcription factors *FOXO1* and *FOXO3*, and the TWEAK receptor Fn14 (*TNFRSF12A*), which are all upstream activators of ubiquitin-mediated proteolysis.

Activation of cardiac fetal gene expression profile. In contrast to the skeletal muscle balancing protein synthesis and degradation to maintain muscle tone and integrity, cardiac tissue shows a distinct mechanism to maintain contractile function and muscle integrity throughout hibernation. This phenotype is the expression of the cardiac fetal gene expression profile, including the expression of several cardiac-specific transcription factors including *NKX2.5*, *NFATc1*, *MEF2A*, *GATA4*, *MYOCD*, and *TBX20* (Fig. 8*B*), during hibernation. Direct downstream targets of these transcription factors regulate basal expression of a spectrum of cardiac genes, several of which are upregulated in TOR/IBA, including *MYH6*, *SLC8A1*, *SLC8A3*, *CHRM2*, the adenosine receptor *ADORA1*, and *ATP2A2* (1). It is well established that the mammalian heart is capable of limited endogenous regeneration (11); however, several examples exist of new cardiomyocyte generation through myogenic differentiation of endogenous stem cells (43, 44) or through proliferation of resident cardiomyocytes (15), but this has not been previously reported as a protective strategy in hibernators.

Table 2. *Pair-wise differential expression*

	APR	IBA	TOR
	Heart		
OCT	296	483	786
TOR	*967*	182	
IBA	749		
	Skeletal muscle		
OCT	524	688	938
TOR	*1,317*	109	
IBA	1085		

Counts of pairwise comparisons of differentially expressed genes in the heart and skeletal muscle throughout the circannual cycle. Pair-wise comparisons were performed using DESeq, and *P* values were filtered to restrict a 50% change between 2 collection points (FDR < 0.05). The largest set of genes are differentially expressed between April active (APR) and torpor (TOR) in both tissues (italics). OCT, October active; IBA, interbout arousal.

Table 3. *DAVID Functional Annotation Clusters for genes differentially expressed relative to APR*

Heart Transcriptome Top 5 DAVID Clusters	Enrichment Score	Genes	Skeletal Muscle Transcriptome Top 5 DAVID Clusters	Enrichment Score	Genes
			OCT:APR		
			Upregulated		
1. Fatty acid metabolism	4.49	22	1. Mitochondrial innner membrane	3.51	24
2. Organelle membrane	4.22	50	2. Mitochondrial outer membrane	3.51	13
3. Peroxisome	3.39	14	3. Mitochondrion	3.44	58
4. Lipid biosynthetic process	3.29	17	4. Metal ion binding	2.85	165
5. Lipid binding	2.94	21	5. Organelle lumen	2.71	88
			Downregulated		
1. Blood vessel development	6.91	27	1. Contractile fiber	7.16	25
2. Response to organic substance	5.23	55	2. Oxidation reduction	5.00	147
3. Cell junction	4.43	35	3. Amino acid catabolism	3.52	13
4. Sequence specific DNA binding	3.91	24	4. Response to organic substance	3.24	62
5. Nitrogen compound biosynthesis	3.68	22	5. FAD	2.94	14
			TOR:APR		
			Upregulated		
1. Peroxisome	5.74	14	1. Mitochondrion/F.A. uptake	4.18	63
2. Cell/membrane fraction	3.97	44	2. Mitochondrial inner membrane	3.46	23
3. Membrane/transmembrane region	3.77	162	3. Fatty acid metabolism	2.99	20
4. Fatty acid metabolism	3.65	17	4. Nucleotide binding	2.45	94
5. Organelle membrane	3.64	45	5. PPAR signaling/F.A. metabolism	2.39	11
			Downregulated		
1. Amine catabolic process	4.33	13	1. Contractile fiber	9.34	25
2. Blood circulation	3.74	15	2. Oxidation reduction	5.71	42
3. Regulation of cell motion	3.58	18	3. Amino acid catabolism	4.36	12
4. Electron carrier activity	3.30	13	4. Mitochondrion/A.A. catabolism	3.44	50
5. Protein dimerization activity	3.18	30	5. Extracellular matrix	3.33	22
			IBA:APR		
			Upregulated		
1. Cofactor binding	2.34	10	1. Mitochondrion	4.18	46
2. Fatty acid metabolism	1.87	7	2. Fatty acid metabolism	3.14	14
3. Lipid binding	1.57	7	3. Cellular respiration	2.53	7
4. Peroxisome	1.28	7	4. FAD	2.42	8
5. Mitochondrion	1.23	17	5. Glucose metabolism	1.75	8
			Downregulated		
1. Blood circulation	2.73	9	1. Contractile fiber	2.99	10
2. Apoptosis	1.83	14	2. Oxidation reduction	2.64	21
3. Regulation of cellular catabolism	1.77	6	3. Response to organic substance	2.52	25
4. Oxidation reduction	1.67	13	4. Extracellular matrix	2.09	14
5. Nucleotide binding	1.63	32	5. Aldo/keto reductase activity	2.06	4

Genes that were differentially expressed in OCT, TOR, and IBA relative to APR were sorted for upregulation and downregulation and submitted to DAVID for functional clustering. The top 5 DAVID clusters for upregulated and downregulated genes are shown for TOR, IBA, and OCT, along with enrichment scores and the number of genes identified in each cluster.

The differential expression of several of these fetal genes are also associated with the pathophysiology of heart failure, more specifically hypertrophy. We see significant increases in expression levels of several genes associated with cardiac hypertrophy including the α-1B adrenergic receptor, *ADRA1B* (27), the TGF-β receptor *TGFBR2* (109), and *Wnt11* (24) in TOR and IBA, as well as the α-1A adrenergic receptor, *ADRA1A* (89), in IBA (Fig. 8*B*). There are also several other genes associated with hypertrophy that are differentially expressed (reviewed in Ref. 12), including the phospholipases *PLCB1* and *PLCD3*, the calcineurin catalytic subunit *PPP3CC*, the mitogen-activated protein kinases *MAP3K5*, *MAP2K3*, and *MAP2K6*, and the secreted glycoprotein *ANGPTL4*, which are all significantly upregulated in the heart in TOR and IBA

relative to APR or OCT. Several hypertrophy-related transcripts, including several forms of the CCAAT/enhancer-binding protein *CEBP*, *CEBPA*, *CEBPB*, and *CEBPD* (15), the regulator of calcineurin *RCAN1* (101), the TGF-β receptor *ACVRL1* (35), and the VEGF receptor *FLT1* (67), are significantly downregulated in TOR and IBA relative to APR.

DISCUSSION

One of the key differences between the heart and the skeletal muscle of the hibernator is their functional demand during the hibernation season. During TOR the heart rate can be as low as 3–10 bpm, while still maintaining normal blood pressure and contractile function required to supply the brain and body with

A Fatty acid metabolism

Functional Category	Fatty Acid Oxidation Enzymes	Tissue	Normalized mRNA Reads			
			April	October	Torpor	IBA
Conversion of long-chain fatty acids to fatty-acyl CoA	FABP3	Heart	16404	12926	23830*	19188
		Skeletal	6821	8509	11787*	12880
	ACOT1	Heart	731	850	1777*	1613
		Skeletal	325	416	717*	822
	ACSL1	Heart	2835	3312	4667*	4160
		Skeletal	2915	3927	5681*	4504
	ACSL3	Heart	113	126	187*	168
		Skeletal	84	82	128*	117
	ACSL4	Heart	250	231	244	264
		Skeletal	316	398	634*	596
	ACSL6	Heart	22	30	37	38
		Skeletal	77	106	114	140
Fatty-acyl CoA mitochondrial transport	CPT1A	Heart	769	819	1838*	1648
		Skeletal	211	132	682*	593
	CPT1B	Heart	9009	9692	9529	8674
		Skeletal	8978	12475	14111	12173
	SLC25A20	Heart	868	982	1414*	1303
		Skeletal	564	770	978*	990
β-oxidation of fatty-acyl CoA	ACADS	Heart	1517	1864	2344*	1990
		Skeletal	859	1444	1688*	1654
	ACADVL	Heart	9373	8978	13665*	12026
		Skeletal	7915	7856	9060	8964
	ACAD10	Heart	473	480	718*	630
		Skeletal	428	356	354	335
	ECH1	Heart	3973	6368	8033*	6598
		Skeletal	5116	6454	8081	7584
	ACOT2	Heart	249	291	504*	454
		Skeletal	99	121	213*	228
	HADHA	Heart	8209	9821	15308*	13681
		Skeletal	4584	7838	10228*	10867
	HADHB	Heart	16328	25286	31139*	28469
		Skeletal	6836	14497	18532*	19168
Branched-chain FA metabolism	ACADSB	Heart	2074	2508	1267*	1155
		Skeletal	781	385	244*	302
Lipotoxicity protection	UCP2	Heart	1152	731	1622*	1947
		Skeletal	85	25	79	83
	UCP3	Heart	342	105	344*	269
		Skeletal	2105	755	2329*	1988
Breakdown H$_2$O$_2$	CAT	Heart	1515	1661	2078	2118
		Skeletal	2256	1820	3049*	3043*
	PRDX5	Heart	2715	3406	3896	3590
		Skeletal	494	776	705	757

B Peroxisomal metabolism

Functional Category	Peroxisomal oxidation Enzymes	Tissue	Normalized mRNA Reads			
			April	October	Torpor	IBA
FA transport	SLC27A1	Heart	282	920	1223	1154
		Skeletal	1440	2298	3754*	3032*
	CD36	Heart	8178	6407	7893	7089
		Skeletal	4241	3956	4195	4590
	ABCD3	Heart	1219	934	1476*	1223*
		Skeletal	337	312	404	400
β-oxidation	HSD17B4	Heart	722	901	857	795
		Skeletal	1093	820	997	1260*
	ACAA1	Heart	555	564	1235*	861*
		Skeletal	293	200	334*	343*
Thiolytic Cleavage	ACOT4	Heart	85	106	192*	178*
		Skeletal	44	48	78	80
Oxidation of unsaturated fats	DECR2	Heart	147	156	224*	214*
		Skeletal	95	92	87	90
	ECH1	Heart	3973	6368	8033*	6598
		Skeletal	5116	6454	8081	7584
α-oxidation	HACL1	Heart	120	151	232*	226
		Skeletal	126	118	147	178*
Other	HSDL2	Heart	1997	2079	3240*	3041*
		Skeletal	1441	2090	2949*	3346*
	MVD	Heart	138	138	214*	178
		Skeletal	242	323	354	313
	EPHX2	Heart	1199	1906	2409*	2147
		Skeletal	459	678	520	582
Peroxisome Biogenesis	PEX19	Heart	450	485	687*	636*
		Skeletal	491	447	482	492

Fig. 5. Evidence supporting a shift to fatty acid metabolism with increased reliance on peroxisomal metabolism. There is differential mRNA expression across the circannual cycle for enzymes involved in various stages of fatty acid metabolism (*A*) and peroxisomal metabolism (*B*). Specific genes are grouped into functional categories, and their tissue-specific read counts are listed. Differential expression is signified by colored shading, with red indicating increased expression relative to APR and green indicating reduced expression relative to APR. *Differential expression relative to OCT by pair-wise comparison. Gene are listed by HGNC designations.

oxygen and metabolites. In contrast, skeletal muscle remains largely inactive during TOR and is able to avoid the detrimental effects of disuse atrophy. Upon rewarming to normothermic conditions during an IBA both tissue types return to normal metabolic and physiological functioning, all within a couple of hours. We used tissues from the same animals for both muscle types, combined with Illumina HiSeq sequencing technologies, to make the most direct comparison between the gene programs of the heart and skeletal muscle during hibernation. This comparative analysis improves on previous transcriptome analyses performed in our lab that relied on subtractive hybridization (7), EST identification (17), or 454 sequencing technologies that used pooled samples and therefore lacked statistical validation of expression levels at any given time point (38).

This study both greatly increased the number of transcripts identified over previous studies and clearly highlights the fact that despite the 99% similarity in expression of protein-coding genes in both tissues, disparate functional requirements during hibernation result in only 369 genes that are differentially expressed in heart and skeletal muscle throughout the circannual cycle (Table 1). The similarity in gene expression profiles between heart and skeletal muscle allowed us to identify new strategies for cold tolerance used by both tissues, through increased peroxisomal fatty acid metabolism (Fig. 5*B*). While the functional divergence between the two tissues shows that oxygen handling, through increased iron uptake and transport, is essential for skeletal muscle maintenance (Fig. 7), re-expression of the fetal cardiac gene expression profile is used by the heart to maintain cardiac muscle (Fig. 8*B*). The depth of the transcriptome allowed us to analyze these phenotypes in more detail than what has previously been reported in heart and skeletal muscle of mammalian hibernators.

Glycolytic Enzymes

Functional Category	Glycolytic enzymes	Tissue	Normalized mRNA Reads			
			April	October	Torpor	IBA
Glycolysis	HK1	Heart	3453	3271	5708*	5708*
		Skeletal	126	77	87	102
	HK2	Heart	169	49	11*	8*
		Skeletal	1782	1909	945*	1032
	GCK	Heart	1108	1024	1810*	1616*
		Skeletal	639	689	349*	399
	GPI	Heart	5149	5218	6535	5678
		Skeletal	12241	11415	10706	11415
	PFKM	Heart	17941	14188	21526*	18471*
		Skeletal	43087	38768	39416	33837
	ALDOA	Heart	21000	20390	23715	20873
		Skeletal	171107	208976	169569	159746
	TPI1	Heart	9257	9214	9371	8650
		Skeletal	18636	17743	14579	14487
	GAPDH	Heart	30227	32020	38194	36988
		Skeletal	126577	124486	97481	89246
	PGK1	Heart	4414	5301	5339	5029
		Skeletal	7451	6892	4881*	5098*
	PGAM2	Heart	1464	2144	2124	1381*
		Skeletal	18533	25663	22517	29423
	ENO1	Heart	2250	1688	2879*	2279*
		Skeletal	1476	763	798	821
	PKM2	Heart	13019	11605	16302	15563
		Skeletal	31445	27431	24740	22905
Glucose Transporter	SLC2A4	Heart	2076	2158	1851	1637
		Skeletal	3382	3596	2562*	2091*

Fig. 6. Opposite expression patterns of glycolytic enzymes in heart and skeletal muscle during hibernation. Enzymes of the glycolytic pathway show increased mRNA expression in the heart, while showing decreased expression in the skeletal muscle. Specific genes are grouped into functional categories and their tissue-specific read counts are listed. Differential expression is signified by colored shading, with red indicating increased expression relative to APR and green indicating reduced expression relative to APR. *Differential expression relative to OCT by pair-wise comparison. Gene names are listed using by designations.

Fuel Utilization

During conditions in which whole body metabolism changes, such as hibernation, the relative contribution of individual substrates to energy production will alter. For example, in rats fasted for 46 h mRNA levels for glucose-handling proteins were reduced by as much as 70%, while transcripts involved in fatty acid transport and metabolism were increased >50%. Additionally, the activity and number of peroxisomes in both heart and skeletal muscle increase during fasting in rats (108). However, when glycogen content was evaluated in the heart and skeletal muscle in fasted rats, glycogen content decreased by >35% in skeletal muscle, while increasing up to 40% in the heart (55). Because hibernation involves a long-term fast meant to conserve energy at a time of limited nutrient availability, we proposed that changes in gene expression similar to fasting are occurring during hibernation and that these changes are specific to maintenance of that particular tissue.

Fatty acid and glucose metabolism. Mammalian hibernators rely almost exclusively on lipid reserves accumulated during summer and fall months, while carbohydrate utilization is drastically reduced (reviewed in Ref. 20). The switch from carbohydrate to fatty acid metabolism is regulated by differential gene expression at multiple levels and shares several gene expression changes with fasting (51, 98), including in-

creased expression of the acyl-CoA dehydrogenases *ACADS*, *ACADVL*, and *ACAD10* (Fig. 5A) and the mitochondrial transport protein *CPT1* (Fig. 4A). These similarities reflect the requirement for fatty acid transport and β-oxidation upon nutrient deprivation and increased circulating fatty acid concentrations.

Key differences between fasting and hibernation, as evidenced by mRNA expression, come from the differences in fatty acid transport proteins. Increased expression of the fatty acid translocase *CD36* is observed in the heart and skeletal muscle during fasting in rats (51, 98), while elevated transcript levels of the fatty acid transport protein *SLC27A1* is observed in the heart and skeletal muscle during hibernation in ground squirrels (Fig. 5B). Studies have shown *SLC27A1* directs fatty acids for oxidation in both heart (23) and skeletal muscle (42), is particularly effective at facilitating long-chain fatty acid transport (25), and is protective against intramuscular lipid

Increased Oxidative Capacity

Functional Category	Increased Oxidative Metabolism	Tissue	Normalized mRNA Reads			
			April	October	Torpor	IBA
TCA Cycle	IDH3A	Heart	3524	3585	4384	4119
		Skeletal	2697	5350	4433	4583
	ACO2	Heart	21232	26954	29783	24770
		Skeletal	16448	24399	17987*	15593*
Upstream signaling promoting oxidative metabolism	THRB	Heart	40	48	38	57
		Skeletal	67	91	106	121
	PPARGC1A	Heart	728	631	477	539
		Skeletal	126	201	146*	175
	PPARGC1B	Heart	140	190	233	234
		Skeletal	77	122	198*	204*
Oxygen delivery to cells	VEGFA	Heart	3465	3808	2865	3047
		Skeletal	1660	2884	1746*	1748*
	VEGFB	Heart	1963	2157	1810	1750
		Skeletal	1108	2172	1674*	1722
Iron-sulfur cluster and heme synthesis	TFRC	Heart	641	1006	744	841
		Skeletal	194	2934	327*	308*
	ISCU	Heart	2349	2896	3327	2899
		Skeletal	1144	1561	1993*	2250*
	ALAS1	Heart	2724	4506	3215	2831*
		Skeletal	854	2751	1017*	981*
	ALAS2	Heart	79	162	67*	162
		Skeletal	11	20	21	19
	HMOX1	Heart	134	82	206*	159*
		Skeletal	383	67	446*	452*
	HMOX2	Heart	667	474	578	495
		Skeletal	492	299	402*	366
	SLC25A28	Heart	124	114	176*	137
		Skeletal	147	158	240*	215
	ABCB6	Heart	681	717	1044*	864
		Skeletal	898	900	1292	1225
Oxygen transport/ reserve within cell	MB	Heart	99613	129552	129554	117787
		Skeletal	64821	114017	87326*	99345
Mitochondrial ADP/ATP Transporters	SLC25A4	Heart	47698	48615	57491	51210
		Skeletal	33596	51613	59720	55883
	SLC25A6	Heart	2487	2864	3642	3362
		Skeletal	2217	2465	3754	4251

Fig. 7. Skeletal muscle shows a sharp increase in oxidative capacity beginning in October. There is differential mRNA expression across the circannual cycle for enzymes and processes responsible for oxygen delivery to and within cells. This differential expression is most prominent in skeletal muscle. Specific genes are grouped into functional categories and their tissue-specific counts are listed. Differential expression is signified by colored shading, with red indicating increased expression relative to APR and green indicating reduced expression relative to APR. *Differential expression relative to OCT by pair-wise comparison. Genes are listed by HGNC designations.

A Protein Turnover

Functional Category	Protein Turnover	Tissue	Normalized mRNA Reads			
			April	October	Torpor	IBA
Protein Synthesis	IGF1	Heart	152	125	151	124
		Skeletal	159	224	491*	288
	IGF2	Heart	225	209	195	198
		Skeletal	87	148	165	179
	AKT1	Heart	941	984	1100	1026
		Skeletal	552	872	897	866
	MTOR	Heart	1573	1169	2028*	1596*
		Skeletal	1120	857	1569*	1272*
	RSPS6KB1	Heart	234	231	271	266
		Skeletal	312	409	486*	531*
Negative regulation of protein synthesis	DDIT4	Heart	502	247	68	209
		Skeletal	2073	508	66*	270
	KLF15	Heart	314	299	85*	128*
		Skeletal	492	349	85*	167
	EIF4EBP1	Heart	182	158	178	151
		Skeletal	277	168	150	185
	IGFBP2	Heart	2	2	3	2
		Skeletal	105	51	17*	20*
	IGFBP7	Heart	1630	1161	1327	969
		Skeletal	525	395	370	335
	MSTN	Heart	2	2	3	1
		Skeletal	111	32	11*	29
Protein degradation	FOXO1	Heart	159	130	144	146
		Skeletal	638	520	246*	249*
	FOXO3	Heart	465	441	274*	285*
		Skeletal	810	651	334*	384*
	TNFRSF12A	Heart	229	96	66	105
		Skeletal	357	130	46	75
	ZFAND5	Heart	1040	672	862	685
		SKM	2487	1246	1069	1158

B Cardiac Fetal Gene Re-expression

Functional Category	Cardiac Fetal Gene Program/ Hypertrophy Genes	Normalized mRNA Reads			
		April	October	Torpor	IBA
Cardiac Transcription Factors	NKX2.5	973	846	1300*	1108*
	GATA4	536	679	864*	689
	MEF2A	402	452	689*	619*
	NFATC1	128	161	199	179
	TBX20	332	543	577	670
	MYOCD	490	613	840*	1120*
Receptors/Ligands	ADRA1A	107	166	108	176
	ADRA1B	104	114	226*	154
	TGFBR2	465	689	763*	764
	ACVRL1	193	177	92*	118*
	FLT1	476	443	223*	261*
	WNT11	84	157	169	155
Calcium Signaling	PLCB1	112	73	178*	167*
	PLCD3	516	722	943	838
	PPP3CC	708	589	980*	811*
	RCAN1	393	303	142*	179
P38 Pathway	MAP3K5	334	363	404	528
	MAP2K3	108	56	114*	103*
	MAP2K6	311	149	243	213
Transcriptional Targets	MYH6	216319	261130	400264*	329608
	MYH7	203074	198332	162345	151046
	SLC8A1	6437	9134	12242*	14340*
	SLC8A3	949	1321	1756*	2116*
	CHRM2	206	400	342*	442
	ADORA1	188	197	429*	340*
	ATP2A2	67401	69148	109815*	84798
	ANGPTL4	125	67	301*	213*
Transport Proteins	ATP1A1	5936	7592	10272*	9348*
	ATP1A3	2352	2988	4067*	3546*
CCAAT/enhancer-binding proteins	CEBPA	215	174	72*	115
	CEBPB	424	327	324	257*
	CEBPD	344	180	70*	128

Fig. 8. Differential expression of protein turnover pathways and re-expression of the cardiac fetal gene expression profile suggests mechanisms of muscle preservation. *A*: pronounced differential expression of skeletal muscle mRNA across the circannual cycle for proteins in various pathways of protein turnover. *B*: gene counts from the heart are shown for re-expression of the cardiac fetal gene expression profile. Specific genes are grouped into functional categories and their tissue-specific read counts are listed. Differential expression is signified by colored shading, with red indicating increased expression relative to APR and green indicating reduced expression relative to APR. *Differential expression relative to OCT by pair-wise comparison. Genes are listed by HGNC designations.

accumulation (42). We postulate the increased expression of *SLC27A1* allows for increased ability to transport unsaturated fats across the membrane and that this is a key difference between fasting and hibernation-associated fasting. Taken together, fasting and hibernation-associated fasting both show similar upregulation of fatty acid metabolism, although differences in enzymes might reflect the greatly increased fat storage prior to hibernation that is not seen in normal fasting.

In addition to altered fatty acid metabolism, we observe distinct regulation of glycolytic enzymes in the heart and skeletal muscle. Transcriptional evidence in support of reduced glucose utilization is seen in the skeletal muscle in TOR, with almost every enzyme in the glycolytic pathway showing decreased transcript levels during hibernation (Fig. 6). Conversely, the heart shows increased transcript levels for almost every enzyme in the glycolytic pathway. This divergent pattern of expression of genes associated with glycolysis may reflect the different functional requirements for each tissue. This increased expression of glycolytic transcripts in the heart during TOR may not reflect glucose utilization during TOR but instead may be a protective mechanism to allow the heart to

rapidly utilize glucose during IBAs. Upon arousal significant increases in energy and oxygen are required to fully perfuse the body with oxygenated blood. The heart's ability to switch its utilization of different substrates under stress is critically important to the survival of the whole organism. This increase in glycolytic enzyme transcripts in the heart during hibernation is in opposition to what is observed in fasting and may be a required cardiac mechanism for protecting the heart during hibernation.

Another mechanism by which the hibernator muscle is protected during hibernation is through the storage and utilization of glycogen reserves. Fasting induces increased glycogen content in the heart, while liver and skeletal muscle showed decreased glycogen content in rats (55). Recent data from our lab showed that glycogen content increases in the heart during TOR and decreases in IBA (Heinis FI, Vermillion KL, Andrews MT, Metzger JM, unpublished observations); however, studies on glycogen content in skeletal muscle during hibernation have not been done in the lab. Given that hibernation is a long-term fast, we believe glycogen content will decrease in the skeletal muscle in TOR, while increasing in the heart, because

similar observations were made in the heart and skeletal muscle of fasted rats (55). This maintenance of cardiac glycogen stores in the heart is an intrinsic ability that protects the heart during long-term fasting and ischemic events such as the IBA.

Peroxisomal fatty acid metabolism. Once fatty acids have been transported into the cell, they are bound by fatty acid binding proteins (FABPs). Levels of FABP transcripts are not significantly changed in fasted animals (51, 98), but FABP3 shows elevated transcript levels in both heart and skeletal muscle in TOR (Fig. 5*A*). Once bound by FABP, long-chain fatty acids are activated for synthesis of cellular lipids, or degradation by β-oxidation, by being converted into fatty acyl-CoA esters by the acyl-CoA synthetases. *ACSL1* and *ASCL3* transcript levels are significantly upregulated in both heart and skeletal muscle in TOR and IBA (Fig. 5*A*). In support of the role for β-oxidation following their activation we see increased expression of several transcripts involved in mitochondrial and peroxisomal oxidation. In animal cells, mitochondria as well as peroxisomes oxidize fatty acids via β-oxidation, with long chain, very long chain, and unsaturated fatty acids being preferentially oxidized by peroxisomes (57, 82).

Short and medium-chain fatty acids are readily permeable across mitochondrial and peroxisomal membranes; however, fatty acyl-CoA esters require the presence of transport proteins. Genetic studies provide evidence for the involvement of the ABC protein superfamily in the peroxisomal import of substrates for β-oxidation (50, 94). We observed elevated transcript levels of the ABC transporter *ABCD3* in the heart during TOR, but no change was observed in any of the ABC transporters in skeletal muscle (Fig. 5*B*). This may reflect increased energy requirements and fatty acid metabolism in the heart during hibernation to maintain cardiac contractility, relative to the inactive skeletal muscle. Once the acyl-CoA ester is inside the cell these esters can undergo β-oxidation, and even though the reactions involved in mitochondrial and peroxisomal β-oxidation are identical, the reactions are catalyzed by distinct genes, with a few exceptions in which a single gene encodes a protein directed to both peroxisomes and mitochondria (reviewed in Ref. 101). The only two peroxisome-specific enzymes involved in straight-chain β-oxidation that are upregulated in hibernation are *HSD17B4*, which is significantly upregulated in IBA in skeletal muscle, and the peroxisomal thiolase *ACAA1*, which shows significantly increased transcript levels in TOR in both heart and skeletal muscle (Fig. 5*B*).

Even though only a few enzymes of the straight-chain β-oxidation pathway are upregulated in hibernation, we also see elevated transcript levels of several auxiliary enzymes that are involved in the oxidation of unsaturated fatty acids (Fig. 5*B*). 2,4-Dienoyl-CoA reductase (*DECR2*) is responsible for degradation of unsaturated enoyl CoA esters having double bonds in even and odd-numbered positions in the peroxisome and is significantly upregulated in the heart, but not skeletal muscle in TOR and IBA (Fig. 5*B*). β-Oxidation of unsaturated fatty acids with a double bond at odd-numbered positions can be metabolized via an NADPH-dependent pathway involving $\Delta^{3,5},\Delta^{2,4}$-Dienoyl-CoA isomerase (*ECH1*) (90). Mammals have one gene encoding this protein, which can be targeted into either mitochondria or peroxisomes (29). *ECH1* is expressed at high levels throughout the circannual cycle but shows significantly elevated transcript levels in TOR in both heart and skeletal muscle (Fig. 5*B*).

Once acetyl-CoAs are generated by β-oxidation they need to be exported to the mitochondria. The export of acetyl-CoAs out of the peroxisome in mammals is thought to be accomplished by either of two systems, a carnitine shuttle or through the export of acetate generated from acetyl-CoA by the action of peroxisomal thioesterases (102). Although there is no evidence to support a peroxisome-specific carnitine shuttling of acetyl-CoAs in this transcriptome, increased transcripts of the peroxisome-specific thioesterase *ACOT4* (48) in heart and skeletal muscle in TOR suggest that CoA esters are hydrolyzed within peroxisomes to yield free acids, which are transported to mitochondria and reactivated to their respective CoA esters for completion of β-oxidation (Fig. 5*B*). The efficient breakdown of long chain and unsaturated fatty acids in the peroxisome allows for a steady supply of medium and short chain fatty acids to the mitochondria where they can be quickly metabolized and converted to ATP throughout hibernation. Increased levels of unsaturated fats in the hibernator allow them to reach and tolerate colder temperatures and increase energy savings (30, 33). This ability to efficiently utilize a large depot of unsaturated fatty acids is a cold-tolerant adaptive mechanism, and although this phenotype is more evident in the heart, which more rapidly utilizes ATP, it is also supplying the skeletal muscle with a more efficient fuel utilization mechanism. In support of peroxisome function as a cold-tolerant mechanism, research in plants found a requirement for peroxisome function in the cold-induction of gene expression that allows for plant freezing tolerance, and survival following dark treatment (26).

Oxidative capacity of skeletal muscle. While many of the genes associated with β-oxidation show a gradual increase through OCT, peaking in hibernation in both heart and skeletal muscle, there is an OCT-specific increase in genes associated with oxygen delivery and transport in the skeletal muscle, which would be necessary for the rapid utilization of these fats for oxidative phosphorylation. The primary method of iron uptake into muscle cells is through the binding of transferrin to transferrin-receptor and its subsequent endocytosis (41). Transferrin-receptor (*TFRC*) shows a 15-fold increase in OCT from APR and then decreases but is still differentially elevated during hibernation in skeletal muscle (Fig. 7). Once iron is in the cell it can be stored in ferritin, transported back out of the cell, or incorporated into various functional proteins, usually in the form of heme (41). Increased transcriptional expression of the rate-limiting enzyme in heme synthesis, *ALAS1*, and decreased expression of heme-degradative enzymes *HMOX1*, *HMOX2*, and *POR* indicate enhanced heme synthesis in OCT. In addition to the mitochondrial cytochromes, heme groups can be incorporated into the oxygen transport protein *MB*. In accordance with previous studies, our transcriptome shows significantly increased *MB* expression in OCT in skeletal muscle, with the protein product likely being maintained throughout hibernation (Fig. 6) (80). In diving mammals that undergo regular acute hypoxic events, *MB* is increased in their skeletal muscles as a means of avoiding anaerobic metabolism and the buildup of lactate (72). The increased MB expression in hibernators likely serves a similar purpose during the rewarming process associated with an IBA. Shivering thermogenesis is an important part of the rewarming process, during which oxygen consumption can be as high as three times normal active levels (95). With such extreme whole body oxygen demand, the muscles run the risk of using oxygen more

rapidly than it can be delivered and resorting to anaerobic metabolism. The importance of remaining aerobic during rewarming is also highlighted in the significantly increased expression of the mitochondrial ADP/ATP transporters *SLC25A4* and *SLC25A6* during hibernation (Fig. 7). Angiogenic factors *VEGFA* and *VEGFB* also show increased expression in OCT further highlighting this preparatory increase in oxygen transport to and within skeletal muscle (Fig. 7).

These changes in oxidative capacity are likely mediated through differential expression of the transcriptional coactivators (TCs) *PPARGC1A* and *PPARGC1B*. These TCs are known to induce the expression of a wide variety of genes related to mitochondrial function, oxidative capacity, and the myosin fiber type transition observed in our data (Fig. 7) and others (8, 62). The differential expression of these TCs correlates with their expected transcriptional targets in such a way to suggest that *PPARGC1A* is more responsible for the physiological transition into hibernation with peak expression in OCT, and *PPARGC1B* playing a role in maintaining the hibernation phenotype with increased expression during TOR and IBA. The role of *PPARGC1A* in hibernation has been recently proposed (106), and our data support these findings, but further research is needed to determine the role of *PPARGC1B* in the hibernation phenotype.

Tissue-specific Muscle Maintenance

Both cardiac and skeletal muscle are highly plastic tissues capable of responding to changes in fuel availability and functional demand. During hibernation, skeletal muscle experiences conditions such as prolonged fasting and disuse. These conditions should promote muscle atrophy, but through unique regulation of protein turnover pathways these animals are able to avoid these detrimental effects. Conditions placed on the heart during hibernation include increased stroke volume, increased peripheral resistance and diastolic pressure (104). These conditions result in a hypertrophic response, and although this response shares many similarities as those observed in pathological conditions, hibernators are able to avoid detrimental effects.

Skeletal muscle maintenance. Under normal conditions, muscle homeostasis is achieved by balancing the continuous processes of protein synthesis and degradation. This balance is regulated by mechanisms integrating a variety of signals including nutrient availability and functional demand. Under conditions of fasting or immobility such as those seen in hibernation, these mechanisms can lead to severe muscle atrophy (14, 61). The amount of inactivity typical of a 10-day TOR bout would, in the nonhibernating rat, result in 16–27% reduction in muscle mass depending on muscle type (78). Hibernators interrupt these long periods of immobility only briefly during IBAs, thus remaining largely immobile for 6 mo. Throughout this time their muscles retain normal morphology and functionality (4). The high-throughput transcriptome data provide a comprehensive view of potential regulatory points in these pathways that hibernators may use to avoid atrophy. The atrophic response of nonhibernator skeletal muscle has been well characterized at the transcriptional level (91). A direct comparison of gene expression patterns of active (APR) versus hibernating (TOR) ground squirrels to active versus immobilized rats reveals a nearly complete lack of the typical atrophic response despite extended disuse in hibernation.

Studies suggest that transcription and translation are halted during TOR (96, 97), implying that the protein synthesis necessary to counteract protein degradation can occur only during an IBA. Our hibernators show increased expression of genes in the IGF-1/AKT/mTOR pathway, which is typical of the hypertrophic response to exercise (74) and is a central mechanism of activating protein synthesis (Fig. 8A). The increased transcriptional expression of the mTOR pathway and reduced expression of its inhibitors, such as *DDIT4* and *KLF15*, support the hypothesis that protein synthesis may be occurring in bursts during the IBAs to counteract the processes of protein degradation, but further investigation at the level of proteins and posttranslational regulation would be needed to confirm the role of this pathway (58). Mechanisms of protein degradation include the ubiquitin proteasome system, the lysosomal autophagy system, and Ca^{2+}-activated proteases (calpains). In models of disuse these pathways are upregulated, resulting in an unbalanced rate of protein turnover eventually leading to atrophy. Our transcriptome data show most of these systems to have stable expression despite the conditions of disuse and fasting. However, many important transcription factors and signaling cascades that eventually lead to the activation of these systems show significantly reduced expression during hibernation.

The FOXO transcription factors are master regulators of a variety of proteolytic systems including the lysosomal autophagy system and the ubiquitin-mediated proteolysis system. AKT and the PGC-1 transcriptional coactivators are known to inhibit FOXO transcriptional activity (84, 92). Their overexpression during hibernation could explain the steady expression of FOXO transcriptional targets despite conditions of immobility and fasting that should lead to their overexpression (14, 61). One such transcriptional target of FOXO transcription factors is the gene *ZFAND5*, which plays a major role in the recognition, delivery, and anchoring of ubiquinated proteins to the proteasome (85). *ZFAND5* shows significantly reduced expression beginning in OCT through the hibernation season (Fig. 8A), demonstrating direct regulation of the rate of protein degradation. NF-κB signaling is another important modulator of muscle atrophy (60). NF-κB activation by the proinflammatory cytokine TNF-like weak inducer of apoptosis (TWEAK) has recently been demonstrated to contribute to the atrophic response by inducing the expression of MuRF1 and Atrogin-1, both E3 ubiquitin ligases. (56). Reduced expression in skeletal muscle of the TWEAK receptor *TNFRSF12A* suggests another method by which these animals reduce the rate of protein degradation during hibernation (Fig. 8A). Through transcriptional regulation at various levels, from major transcription factors to cytokines to proteasome anchoring proteins, these animals seem able to maintain a normal rate of protein turnover under otherwise atrophic conditions and preserve muscle function and mass.

Cardiac muscle maintenance. Strong evidence from the transcriptome reveals expression of the fetal gene expression profile as a cardiac-specific mechanism for maintaining cardiac muscle during hibernation. The group of transcription factors, including *NFAT*, *GATA4*, *NKX2.5*, *MEF2A*, and *TBX20*, which are all significantly upregulated during torpor (Fig. 8B), are all critical factors involved in heart development (36, 39, 40, 77).

This suite of cardiac transcription factors are essential transcriptional activators that are expressed predominantly in the myocardium and regulate the expression of the cardiac genes encoding structural and/or regulatory proteins characteristic of cardiomyocytes. Expression of these genes during hibernation suggests the possibility of regenerative capabilities of heart muscle, but these transcription factors are also recognized for more than just their role in cardiogenesis. In the postnatal myocardium, many major pathways for pathological remodeling converge on this set of transcription factors, several of which are associated with cardiac hypertrophy and heart failure (10, 31, 76).

The hibernator heart exhibits a hypertrophic response as a result of increased stroke volume, peripheral resistance, and diastolic pressure (104). However, the hypertrophic response to hibernation shares characteristics of both physiological and pathological hypertrophy. Physiological hypertrophy increases myocyte size by increased growth factor signaling, typically through the IGF/PI3K/AKT pathway, resulting in increased protein synthesis that is mediated by thyroid hormone signaling (reviewed in Ref. 12). While in TOR, expression levels of the receptors *IGFR1* and *PI3KR*, and *AKT* are all significantly decreased, highlighting a major difference between physiological and hibernation related hypertrophy. The best characterized signaling cascade mediating pathological hypertrophy is Gαq signaling, downstream of GPCRs, and is activated by angiotensin-II (*AGT*), endothelin-1 (*EDN1*), and catecholamines. The expression of *AGT* and *EDN1* and their receptors does not show significant changes throughout the year; however, large fluctuations in several of the catecholamine receptors are significantly altered throughout the hibernation season (Fig. 8*B*). This alteration in adrenergic signaling is a likely mechanism by which hibernators exhibit a hypertrophic response without developing heart failure.

Adrenergic signaling through α-adrenergic receptors is responsible for mobilizing intracellular calcium via a PLC/IP$_3$ mechanism (66). We see increased mRNA expression of *ADRA1B* in TOR, along with two PLC transcript variants, *PLCB1* and *PLCD3* (Fig. 8*B*). PLC cleaves phosphatidylinositol 4,5-diphosphate to yield IP$_3$ and DAG. IP$_3$ interacts with the sarcoplasmic reticulum to release stored Ca^{2+}. In addition to mobilizing calcium from intracellular stores, activation of PLC influences intracellular Ca^{2+} by inhibition of L-type Ca^{2+} channels or by activation of Ca^{2+} channels, Na$^+$-H$^+$, and Na$^+$-Ca^{2+} exchangers (67, 68). During hibernation the Na$^+$-Ca^{2+} exchangers *SLC8A1* and *SLC8A3* are both significantly increased along with the Na$^+$-K$^+$ transporters *ATP1A1* and *ATP1A3* (Fig. 8*B*). Increased intracellular calcium also activates the calcineurin-dependent transcriptional pathway that is typically associated with the fetal gene expression profile and cardiac hypertrophy. Ca^{2+}-dependent calcineurin signaling removes the phosphate group from NFAT, allowing for translocation into the nucleus, where NFAT activates GATA4, and in cooperation with MEF2 is responsible for activation of the cardiac fetal gene expression profile, or cardiac transcription (69).

We also see increased expression of the transcription factors *NKX2.5*, *MYOCD*, and *TBX20* (Fig. 8*B*), which are important in the differentiation, proliferation, and maturation of the heart (47, 79, 87). These transcription factors are important for regulating a large number of cardiac remodeling genes. Expression of the cardiac fetal gene expression profile is often characterized by the increase in ANP, BNP, α-skeletal actin (ACTA1), and alterations of α- and β-myosin heavy chains (MYH6 and MHY7, respectively) (12, 49). Our transcriptome data do not show an increase in *ANP* transcript levels, did not identify *BNP*, and show significantly decreased transcript levels of *ACTA1*. We also observe the opposite pattern of myosin heavy chain isoform expression, with *MYH6* increasing, while *MYH7* decreases (Fig. 8*B*). This switch to the α-myosin heavy chain *MYH6* is likely important for maintaining contractile function during hibernation, with α-myosin heavy chains allowing for greater force contractility. This increase in *MYH6* was previously observed (70), and we propose this to be important for continuous pumping of blood with higher viscosity due to decreased temperature. These dissimilarities between the fetal gene expression profile in pathological hypertrophy versus that seen in hibernation are likely important for maintaining cardiac function without progressing to cardiac dysfunction and heart failure.

Similar to what is seen in physiological hypertrophy, we observe decreased transcript levels of several of the CCAT-enhancer binding proteins (CEBP) in TOR and IBA (Fig. 8*B*). The downregulation of *CEBPB* permits the expression of beneficial or protective genes and allows for expression of genes that enhance cardiomyocyte proliferation and therefore cell number in the heart in exercised mice and shows that CEBPB is an important regulator of adaptive or physiological hypertrophy (15). The expression of fetal cardiac genes, the potential for a proliferative phenotype mediated by ADRA1A, and the reduced CEBP expression highlight the importance of further studies to determine if the hypertrophic response is due to increased muscle fiber size or cardiomyocyte proliferation. Additionally, pathological and physiological hypertrophy are associated with distinct metabolic profiles. Substrate utilization in pathological hypertrophy resembles that of the fetal heart, which are characterized by decreased fatty acid oxidation and increased glucose oxidation, while physiological hypertrophy is associated with increased fatty acid and glucose oxidation (59). Evidence from the cardiac transcriptome (19), proteome (83), and metabolic labeling (6) shows that the hibernator heart is increasing fatty acid oxidation and glycolysis without increasing glucose oxidation. The ability of the hibernator to respond to the stress of hibernation with a combination of physiological and pathological hypertrophic responses might be the key to preventing heart failure and maintaining contractile function throughout temperature extremes. Also the nature of repeated IBAs and alteration of adrenergic signaling likely allow for protection of the heart through preventing insulin sensitivity and fatty acid lipotoxicity, while allowing for critical protein synthesis. Further in-depth analysis of the proteome of heart and skeletal muscle would complement this work to correlate with mRNA expression and confirm altered signaling and adaptive mechanisms for survival during hibernation.

Conclusion

Transcriptomic analysis of the heart and skeletal muscle has revealed tissue-specific mechanisms by which these two striated muscles function under the extreme conditions of mammalian hibernation. Our data suggest similar mechanisms of increased fatty acid and peroxisomal metabolism used by both

tissues, while hibernator hearts are able to resort to glucose metabolism in times of need. Additionally, skeletal muscle shows an early increase in oxidative capacity necessary for the altered fuel utilization and oxygen demand of shivering. These two muscles show disparate mechanisms by which they maintain their morphology and functionality during hibernation. Skeletal muscle exhibits unique regulation of pathways involved in protein turnover as a means of preserving muscle proteins and avoiding atrophy, while the heart reverts to the fetal gene expression profile, but is able to avoid the cardiac hypertrophy and heart failure usually associated with these conditions. While there are very similar metabolic demands on these two muscle tissues, their diverse functional requirements are highlighted in the very different mechanisms by which they maintain functionality throughout the circannual cycle.

DISCLOSURES

No conflicts of interest, financial or otherwise, are declared by the author(s).

AUTHOR CONTRIBUTIONS

Author contributions: K.L.V., K.J.A., and M.H. analyzed data; K.L.V., K.J.A., and M.H. interpreted results of experiments; K.L.V. and K.J.A. prepared figures; K.L.V. and K.J.A. drafted manuscript; K.L.V., K.J.A., M.H., and M.T.A. edited and revised manuscript; K.L.V., K.J.A., M.H., and M.T.A. approved final version of manuscript; M.H. and M.T.A. conception and design of research.

REFERENCES

1. **Akazawa H, Komuro I.** Roles of cardiac transcription factors in cardiac hypertrophy. *Circ Res* 92: 1079–1088, 2003.
2. **Altschul SF, Madden TL, Schaffer AA, Zhang J, Zhang Z, Miller W, Lipman DJ.** Gapped BLAST and PSI-BLAST: a new generation of protein database search programs. *Nucleic Acids Res* 25: 3389–3402, 1997.
3. **Anders S, Huber W.** Differential expression analysis for sequence count data. *Genome Biol* 11: R106, 2010.
4. **Andres-Mateos E, Brinkmeier H, Burks TN, Mejias R, Files DC, Steinberger M, Soleimani A, Marx R, Simmers JL, Lin B, Finanger Hedderick E, Marr TG, Lin BM, Hourde C, Leinwand LA, Kuhl D, Foller M, Vogelsang S, Hernandez-Diaz I, Vaughan DK, Alvarez de la Rosa D, Lang F, Cohn RD.** Activation of serum/glucocorticoid-induced kinase 1 (SGK1) is important to maintain skeletal muscle homeostasis and prevent atrophy. *EMBO Mol Med* 5: 80–91, 2013.
5. **Andrews MT.** Advances in molecular biology of hibernation in mammals. *Bioessays* 29: 431–440, 2007.
6. **Andrews MT, Russeth KP, Drewes LR, Henry PG.** Adaptive mechanisms regulate preferred utilization of ketones in the heart and brain of a hibernating mammal during arousal from torpor. *Am J Physiol Regul Integr Comp Physiol* 296: R383–R393, 2009.
7. **Andrews MT, Squire TL, Bowen CM, Rollins MB.** Low-temperature carbon utilization is regulated by novel gene activity in the heart of a hibernating mammal. *Proc Natl Acad Sci USA* 95: 8392–8397, 1998.
8. **Arany Z, Foo SY, Ma Y, Ruas JL, Bommi-Reddy A, Girnun G, Cooper M, Laznik D, Chinsomboon J, Rangwala SM, Baek KH, Rosenzweig A, Spiegelman BM.** HIF-independent regulation of VEGF and angiogenesis by the transcriptional coactivator PGC-1alpha. *Nature* 451: 1008–1012, 2008.
9. **Bassel-Duby R, Olson EN.** Signaling pathways in skeletal muscle remodeling. *Annu Rev Biochem* 75: 19–37, 2006.
10. **Belke DD, Milner RE, Wang LC.** Seasonal variations in the rate and capacity of cardiac SR calcium accumulation in a hibernating species. *Cryobiology* 28: 354–363, 1991.
11. **Bergmann O, Bhardwaj RD, Bernard S, Zdunek S, Barnabe-Heider F, Walsh S, Zupicich J, Alkass K, Buchholz BA, Druid H, Jovinge S, Frisen J.** Evidence for cardiomyocyte renewal in humans. *Science* 324: 98–102, 2009.
12. **Bernardo BC, Weeks KL, Pretorius L, McMullen JR.** Molecular distinction between physiological and pathological cardiac hypertrophy: experimental findings and therapeutic strategies. *Pharmacol Therapeut* 128: 191–227, 2010.
13. **Biorck G, Johansson B, Schmid H.** Reactions of hedgehogs, hibernating and non-hibernating, to the inhalation of oxygen, carbon dioxide and nitrogen. *Acta Physiol Scand* 37: 71–83, 1956.
14. **Booth FW.** Effect of limb immobilization on skeletal muscle. *J Appl Physiol Respir Environ Exerc Physiol* 52: 1113–1118, 1982.
15. **Bostrom P, Mann N, Wu J, Quintero PA, Plovie ER, Panakova D, Gupta RK, Xiao C, MacRae CA, Rosenzweig A, Spiegelman BM.** C/EBPbeta controls exercise-induced cardiac growth and protects against pathological cardiac remodeling. *Cell* 143: 1072–1083, 2010.
16. **Bourgon R, Gentleman R, Huber W.** Independent filtering increases detection power for high-throughput experiments. *Proc Natl Acad Sci USA* 107: 9546–9551, 2010.
17. **Brauch KM, Dhruv ND, Hanse EA, Andrews MT.** Digital transcriptome analysis indicates adaptive mechanisms in the heart of a hibernating mammal. *Physiol Genomics* 23: 227–234, 2005.
18. **Breton S.** The cellular physiology of carbonic anhydrases. *J Pancreas* 2: 159–164, 2001.
19. **Buck MJ, Squire TL, Andrews MT.** Coordinate expression of the PDK4 gene: a means of regulating fuel selection in a hibernating mammal. *Physiol Genomics* 8: 5–13, 2002.
20. **Carey HV, Andrews MT, Martin SL.** Mammalian hibernation: cellular and molecular responses to depressed metabolism and low temperature. *Physiol Rev* 83: 1153–1181, 2003.
21. **Carriere V, Barbat A, Rousset M, Brot-Laroche E, Dussaulx E, Cambier D, De Waziers ID, Beaune P, Zweibaum A.** Regulation of sucrase-isomaltase and hexose transporters in Caco-2 cells: a role for cytochrome P-4501A1? *Am J Physiol Gastrointest Liver Physiol* 270: G976–G986, 1996.
22. **Carriere V, Rodolosse A, Lacasa M, Cambier D, Zweibaum A, Rousset M.** Hypoxia and CYP1A1 induction-dependent regulation of proteins involved in glucose utilization in Caco-2 cells. *Am J Physiol Gastrointest Liver Physiol* 274: G1101–G1108, 1998.
23. **Chiu HC, Kovacs A, Blanton RM, Han X, Courtois M, Weinheimer CJ, Yamada KA, Brunet S, Xu H, Nerbonne JM, Welch MJ, Fettig NM, Sharp TL, Sambandam N, Olson KM, Ory DS, Schaffer JE.** Transgenic expression of fatty acid transport protein 1 in the heart causes lipotoxic cardiomyopathy. *Circ Res* 96: 225–233, 2005.
24. **Dawson K, Aflaki M, Nattel S.** Role of the Wnt-Frizzled system in cardiac pathophysiology: a rapidly developing, poorly understood area with enormous potential. *J Physiol* 591: 1409–1432, 2013.
25. **DiRusso CC, Li H, Darwis D, Watkins PA, Berger J, Black PN.** Comparative biochemical studies of the murine fatty acid transport proteins (FATP) expressed in yeast. *J Biol Chem* 280: 16829–16837, 2005.
26. **Dong CH, Zolman BK, Bartel B, Lee BH, Stevenson B, Agarwal M, Zhu JK.** Disruption of Arabidopsis CHY1 reveals an important role of metabolic status in plant cold stress signaling. *Mol Plant* 2: 59–72, 2009.
27. **Du XJ.** Distinct role of adrenoceptor subtypes in cardiac adaptation to chronic pressure overload. *Clin Exp Pharmacol Physiol* 35: 355–360, 2008.
28. **Fawcett DW, Lyman CP.** The effect of low environmental temperature on the composition of depot fat in relation to hibernation. *J Physiol* 126: 235–247, 1954.
29. **Filppula SA, Yagi AI, Kilpelainen SH, Novikov D, FitzPatrick DR, Vihinen M, Valle D, Hiltunen JK.** Delta3,5-delta2,4-dienoyl-CoA isomerase from rat liver. Molecular characterization. *J Biol Chem* 273: 349–355, 1998.
30. **Florant GL, Hester L, Ameenuddin S, Rintoul DA.** The effect of a low essential fatty acid diet on hibernation in marmots. *Am J Physiol Regul Integr Comp Physiol* 264: R747–R753, 1993.

31. **Frey N, Olson EN.** Cardiac hypertrophy: the good, the bad, and the ugly. *Annu Rev Physiol* 65: 45–79, 2003.

32. **Garnier A, Fortin D, Delomenie C, Momken I, Veksler V, Ventura-Clapier R.** Depressed mitochondrial transcription factors and oxidative capacity in rat failing cardiac and skeletal muscles. *J Physiol* 551: 491–501, 2003.

33. **Geiser F, Kenagy GJ.** Polyunsaturated lipid diet lengthens torpor and reduces body temperature in a hibernator. *Am J Physiol Regul Integr Comp Physiol* 252: R897–R901, 1987.

34. **Grabek KR, Karimpour-Fard A, Epperson LE, Hindle A, Hunter LE, Martin SL.** Multistate proteomics analysis reveals novel strategies used by a hibernator to precondition the heart and conserve ATP for winter heterothermy. *Physiol Genomics* 43: 1263–1275, 2011.

35. **Grabherr MG, Haas BJ, Yassour M, Levin JZ, Thompson DA, Amit I, Adiconis X, Fan L, Raychowdhury R, Zeng Q, Chen Z, Mauceli E, Hacohen N, Gnirke A, Rhind N, di Palma F, Birren BW, Nusbaum C, Lindblad-Toh K, Friedman N, Regev A.** Full-length transcriptome assembly from RNA-Seq data without a reference genome. *Nat Biotechnol* 29: 644–652, 2011.

36. **Greulich F, Rudat C, Kispert A.** Mechanisms of T-box gene function in the developing heart. *Cardiovasc Res* 91: 212–222, 2011.

37. **Hampton M, Melvin RG, Andrews MT.** Transcriptomic analysis of brown adipose tissue across the physiological extremes of natural hibernation. *PLoS One* 8: e85157, 2013.

38. **Hampton M, Melvin RG, Kendall AH, Kirkpatrick BR, Peterson N, Andrews MT.** Deep sequencing the transcriptome reveals seasonal adaptive mechanisms in a hibernating mammal. *PLoS One* 6: e27021, 2011.

39. **Harvey RP.** Patterning the vertebrate heart. *Nat Rev Genet* 3: 544–556, 2002.

40. **He A, Kong SW, Ma Q, Pu WT.** Co-occupancy by multiple cardiac transcription factors identifies transcriptional enhancers active in heart. *Proc Natl Acad Sci USA* 108: 5632–5637, 2011.

41. **Hentze MW, Muckenthaler MU, Andrews NC.** Balancing acts: molecular control of mammalian iron metabolism. *Cell* 117: 285–297, 2004.

42. **Holloway GP, Chou CJ, Lally J, Stellingwerff T, Maher AC, Gavrilova O, Haluzik M, Alkhateeb H, Reitman ML, Bonen A.** Increasing skeletal muscle fatty acid transport protein 1 (FATP1) targets fatty acids to oxidation and does not predispose mice to diet-induced insulin resistance. *Diabetologia* 54: 1457–1467, 2011.

43. **Hosoda T, D'Amario D, Cabral-Da-Silva MC, Zheng H, Padin-Iruegas ME, Ogorek B, Ferreira-Martins J, Yasuzawa-Amano S, Amano K, Ide-Iwata N, Cheng W, Rota M, Urbanek K, Kajstura J, Anversa P, Leri A.** Clonality of mouse and human cardiomyogenesis in vivo. *Proc Natl Acad Sci USA* 106: 17169–17174, 2009.

44. **Hsieh PC, Segers VF, Davis ME, MacGillivray C, Gannon J, Molkentin JD, Robbins J, Lee RT.** Evidence from a genetic fate-mapping study that stem cells refresh adult mammalian cardiomyocytes after injury. *Nat Med* 13: 970–974, 2007.

45. **Huang da W, Sherman BT, Stephens R, Baseler MW, Lane HC, Lempicki RA.** DAVID gene ID conversion tool. *Bioinformation* 2: 428–430, 2008.

46. **Huang da W, Sherman BT, Tan Q, Collins JR, Alvord WG, Roayaei J, Stephens R, Baseler MW, Lane HC, Lempicki RA.** The DAVID Gene Functional Classification Tool: a novel biological module-centric algorithm to functionally analyze large gene lists. *Genome Biol* 8: R183, 2007.

47. **Huang J, Elicker J, Bowens N, Liu X, Cheng L, Cappola TP, Zhu X, Parmacek MS.** Myocardin regulates BMP10 expression and is required for heart development. *J Clin Invest* 122: 3678–3691, 2012.

48. **Hunt MC, Siponen MI, Alexson SE.** The emerging role of acyl-CoA thioesterases and acyltransferases in regulating peroxisomal lipid metabolism. *Biochim Biophys Acta* 1822: 1397–1410, 2012.

49. **Iemitsu M, Miyauchi T, Maeda S, Sakai S, Kobayashi T, Fujii N, Miyazaki H, Matsuda M, Yamaguchi I.** Physiological and pathological cardiac hypertrophy induce different molecular phenotypes in the rat. *Am J Physiol Regul Integr Comp Physiol* 281: R2029–R2036, 2001.

50. **Imanaka T, Aihara K, Takano T, Yamashita A, Sato R, Suzuki Y, Yokota S, Osumi T.** Characterization of the 70-kDa peroxisomal membrane protein, an ATP binding cassette transporter. *J Biol Chem* 274: 11968–11976, 1999.

51. **Jagoe RT, Lecker SH, Gomes M, Goldberg AL.** Patterns of gene expression in atrophying skeletal muscles: response to food deprivation. *FASEB J* 16: 1697–1712, 2002.

52. **Johansson BW.** Heart and circulation in hibernators. *Mammalian Hibernation III*, edited by Fisher KC. New York: Oliver & Boyd, 1967, p. 200–218.

53. **Johansson BW.** The hibernator heart–nature's model of resistance to ventricular fibrillation. *Cardiovasc Res* 31: 826–832, 1996.

54. **Johansson BW.** Temperature dependence of cholinesterase and lactate dehydrogenase in the guinea-pig, hedgehog and codfish. *Acta Physiol Scand* 77: 1–6, 1969.

55. **Kokubun E, Hirabara SM, Fiamoncini J, Curi R, Haebisch H.** Changes of glycogen content in liver, skeletal muscle, and heart from fasted rats. *Cell Biochem Funct* 27: 488–495, 2009.

56. **Kumar A, Bhatnagar S, Paul PK.** TWEAK and TRAF6 regulate skeletal muscle atrophy. *Curr Opin Clin Nutr Metab Care* 15: 233–239, 2012.

57. **Lazarow PB, De Duve C.** A fatty acyl-CoA oxidizing system in rat liver peroxisomes; enhancement by clofibrate, a hypolipidemic drug. *Proc Natl Acad Sci USA* 73: 2043–2046, 1976.

58. **Lee K, So H, Gwag T, Ju H, Lee JW, Yamashita M, Choi I.** Molecular mechanism underlying muscle mass retention in hibernating bats: role of periodic arousal. *J Cell Physiol* 222: 313–319, 2010.

59. **Lehman JJ, Kelly DP.** Gene regulatory mechanisms governing energy metabolism during cardiac hypertrophic growth. *Heart Fail Rev* 7: 175–185, 2002.

60. **Li H, Malhotra S, Kumar A.** Nuclear factor-kappa B signaling in skeletal muscle atrophy. *J Mol Med* 86: 1113–1126, 2008.

61. **Li JB, Goldberg AL.** Effects of food deprivation on protein synthesis and degradation in rat skeletal muscles. *Am J Physiol* 231: 441–448, 1976.

62. **Lin J, Handschin C, Spiegelman BM.** Metabolic control through the PGC-1 family of transcription coactivators. *Cell Metab* 1: 361–370, 2005.

63. **Liu B, Belke DD, Wang LC.** Ca^{2+} uptake by cardiac sarcoplasmic reticulum at low temperature in rat and ground squirrel. *Am J Physiol Regul Integr Comp Physiol* 272: R1121–R1127, 1997.

64. **Luque A, Carpizo DR, Iruela-Arispe ML.** ADAMTS1/METH1 inhibits endothelial cell proliferation by direct binding and sequestration of VEGF165. *J Biol Chem* 278: 23656–23665, 2003.

65. **Lyman CP, O'Brien RC.** Autonomic control of circulation during the hibernating cycle in ground squirrels. *J Physiol* 168: 477–499, 1963.

66. **Minneman KP.** Alpha 1-adrenergic receptor subtypes, inositol phosphates, and sources of cell Ca^{2+}. *Pharmacol Rev* 40: 87–119, 1988.

67. **Minneman KP, Esbenshade TA.** Alpha 1-adrenergic receptor subtypes. *Annu Rev Pharmacol Toxicol* 34: 117–133, 1994.

68. **Minneman KP, Han C, Abel PW.** Comparison of alpha 1-adrenergic receptor subtypes distinguished by chlorethylclonidine and WB 4101. *Mol Pharmacol* 33: 509–514, 1988.

69. **Molkentin JD, Lu JR, Antos CL, Markham B, Richardson J, Robbins J, Grant SR, Olson EN.** A calcineurin-dependent transcriptional pathway for cardiac hypertrophy. *Cell* 93: 215–228, 1998.

70. **Nelson OL, Rourke BC.** Increase in cardiac myosin heavy-chain (MyHC) alpha protein isoform in hibernating ground squirrels, with echocardiographic visualization of ventricular wall hypertrophy and prolonged contraction. *J Exp Biol* 216: 4678–4690, 2013.

71. **Nielsen KC, Owman C.** Difference in cardiac adrenergic innervation between hibernators and non-hibernating mammals. *Acta Physiol Scand Suppl* 316: 1–30, 1968.

72. **Noren SR, Williams TM.** Body size and skeletal muscle myoglobin of cetaceans: adaptations for maximizing dive duration. *Comp Biochem Physiol A Mol Integr Physiol* 126: 181–191, 2000.

73. **Nowell MM, Choi H, Rourke BC.** Muscle plasticity in hibernating ground squirrels (Spermophilus lateralis) is induced by seasonal, but not low-temperature, mechanisms. *J Comp Physiol B* 181: 147–164, 2011.

74. **Ochi E, Ishii N, Nakazato K.** Time course change of IGF1/Akt/mTOR/p70s6k Pathway activation in rat gastrocnemius muscle during repeated bouts of eccentric exercise. *J Sports Sci Med* 9: 170–175, 2010.

75. **Okey AB.** Enzyme induction in the cytochrome P-450 system. *Pharmacol Therapeut* 45: 241–298, 1990.

76. **Olson EN, Schneider MD.** Sizing up the heart: development redux in disease. *Genes Dev* 17: 1937–1956, 2003.

77. **Peterkin T, Gibson A, Loose M, Patient R.** The roles of GATA-4, -5 and -6 in vertebrate heart development. *Sem Cell Dev Biol* 16: 83–94, 2005.

78. **Phillips SM, Glover EI, Rennie MJ.** Alterations of protein turnover underlying disuse atrophy in human skeletal muscle. *J Appl Physiol* 107: 645–654, 2009.

79. **Plageman TF Jr, Yutzey KE.** T-box genes and heart development: putting the "T" in heart. *Dev Dyn* 232: 11–20, 2005.

80. **Postnikova GB, Tselikova SV, Kolaeva SG, Solomonov NG.** Myoglobin content in skeletal muscles of hibernating ground squirrels rises in autumn and winter. *Comp Biochem Physiol A Mol Integr Physiol* 124: 35–37, 1999.

81. **Pownall ME, Gustafsson MK, Emerson CP Jr.** Myogenic regulatory factors and the specification of muscle progenitors in vertebrate embryos. *Annu Rev Cell Dev Biol* 18: 747–783, 2002.

82. **Reddy JK, Mannaerts GP.** Peroxisomal lipid metabolism. *Annu Rev Nutr* 14: 343–370, 1994.

83. **Russeth KP, Higgins L, Andrews MT.** Identification of proteins from non-model organisms using mass spectrometry: application to a hibernating mammal. *J Proteome Res* 5: 829–839, 2006.

84. **Sandri M, Lin J, Handschin C, Yang W, Arany ZP, Lecker SH, Goldberg AL, Spiegelman BM.** PGC-1alpha protects skeletal muscle from atrophy by suppressing FoxO3 action and atrophy-specific gene transcription. *Proc Natl Acad Sci USA* 103: 16260–16265, 2006.

85. **Schiaffino S, Dyar KA, Ciciliot S, Blaauw B, Sandri M.** Mechanisms regulating skeletal muscle growth and atrophy. *FEBS J* 280: 4294–4314, 2013.

86. **Schiaffino S, Reggiani C.** Fiber types in mammalian skeletal muscles. *Physiol Rev* 91: 1447–1531, 2011.

87. **Schlesinger J, Schueler M, Grunert M, Fischer JJ, Zhang Q, Krueger T, Lange M, Tonjes M, Dunkel I, Sperling SR.** The cardiac transcription network modulated by Gata4, Mef2a, Nkx2.5, Srf, histone modifications, and microRNAs. *PLoS Genet* 7: e1001313, 2011.

88. **Schwartz C, Hampton M, Andrews MT.** Seasonal and regional differences in gene expression in the brain of a hibernating mammal. *PLoS One* 8: e58427, 2013.

89. **Simpson PC, Kariya K, Karns LR, Long CS, Karliner JS.** Adrenergic hormones and control of cardiac myocyte growth. *Mol Cell Biochem* 104: 35–43, 1991.

90. **Smeland TE, Nada M, Cuebas D, Schulz H.** NADPH-dependent beta-oxidation of unsaturated fatty acids with double bonds extending from odd-numbered carbon atoms. *Proc Natl Acad Sci USA* 89: 6673–6677, 1992.

91. **Stevenson EJ, Giresi PG, Koncarevic A, Kandarian SC.** Global analysis of gene expression patterns during disuse atrophy in rat skeletal muscle. *J Physiol* 551: 33–48, 2003.

92. **Stitt TN, Drujan D, Clarke BA, Panaro F, Timofeyva Y, Kline WO, Gonzalez M, Yancopoulos GD, Glass DJ.** The IGF-1/PI3K/Akt pathway prevents expression of muscle atrophy-induced ubiquitin ligases by inhibiting FOXO transcription factors. *Mol Cell* 14: 395–403, 2004.

93. **Thauer R.** The circulation in hypothermia of nonhibernating animals and man. In: *Handbook of Physiology*. Washington DC: Am Physiol Soc, 1965, p. 1899–1920.

94. **Theodoulou FL, Holdsworth M, Baker A.** Peroxisomal ABC transporters. *FEBS Lett* 580: 1139–1155, 2006.

95. **Toien O, Drew KL, Chao ML, Rice ME.** Ascorbate dynamics and oxygen consumption during arousal from hibernation in Arctic ground squirrels. *Am J Physiol Regul Integr Comp Physiol* 281: R572–R583, 2001.

96. **van Breukelen F, Martin SL.** Reversible depression of transcription during hibernation. *J Comp Physiol B* 172: 355–361, 2002.

97. **van Breukelen F, Martin SL.** Translational initiation is uncoupled from elongation at 18 degrees C during mammalian hibernation. *Am J Physiol Regul Integr Comp Physiol* 281: R1374–R1379, 2001.

98. **Van der Lee KA, Willemsen PH, Samec S, Seydoux J, Dulloo AG, Pelsers MM, Glatz JF, Van der Vusse GJ, Van Bilsen M.** Fasting-induced changes in the expression of genes controlling substrate metabolism in the rat heart. *J Lipid Res* 42: 1752–1758, 2001.

99. **Vazquez F, Hastings G, Ortega MA, Lane TF, Oikemus S, Lombardo M, and Iruela-Arispe ML.** METH-1, a human ortholog of ADAMTS-1, and METH-2 are members of a new family of proteins with angio-inhibitory activity. *J Biol Chem* 274: 23349–23357, 1999.

100. **Veiga-da-Cunha M, Chevalier N, Stroobant V, Vertommen D, Van Schaftingen E.** Metabolite proofreading in carnosine and homocarnosine synthesis: molecular identification of PM20D2 as beta-alanyl-lysine dipeptidase. *J Biol Chem* 289: 19726–19736, 2014.

101. **Wanders RJ, Vreken P, Ferdinandusse S, Jansen GA, Waterham HR, van Roermund CW, Van Grunsven EG.** Peroxisomal fatty acid alpha- and beta-oxidation in humans: enzymology, peroxisomal metabolite transporters and peroxisomal diseases. *Biochem Soc Transact* 29: 250–267, 2001.

102. **Wanders RJ, Waterham HR.** Biochemistry of mammalian peroxisomes revisited. *Annu Rev Biochem* 75: 295–332, 2006.

103. **Wang SQ, Lakatta EG, Cheng H, Zhou ZQ.** Adaptive mechanisms of intracellular calcium homeostasis in mammalian hibernators. *J Exp Biol* 205: 2957–2962, 2002.

104. **Wickler SJ, Hoyt DF, van Breukelen F.** Disuse atrophy in the hibernating golden-mantled ground squirrel, Spermophilus lateralis. *Am J Physiol Regul Integr Comp Physiol* 261: R1214–R1217, 1991.

105. **Wu CW, Storey KB.** Regulation of the mTOR signaling network in hibernating thirteen-lined ground squirrels. *J Exp Biol* 215: 1720–1727, 2012.

106. **Xu R, Andres-Mateos E, Mejias R, MacDonald EM, Leinwand LA, Merriman DK, Fink RH, Cohn RD.** Hibernating squirrel muscle activates the endurance exercise pathway despite prolonged immobilization. *Exp Neurol* 247: 392–401, 2013.

107. **Yatani A, Kim SJ, Kudej RK, Wang Q, Depre C, Irie K, Kranias EG, Vatner SF, Vatner DE.** Insights into cardioprotection obtained from study of cellular Ca^{2+} handling in myocardium of true hibernating mammals. *Am J Physiol Heart Circ Physiol* 286: H2219–H2228, 2004.

108. **Yokota S, Asayama K.** Peroxisomes of the rat cardiac and soleus muscles increase after starvation. A biochemical and immunocytochemical study. *Histochemistry* 93: 287–293, 1990.

109. **Ziyadeh FN.** Mediators of diabetic renal disease: the case for tgf-Beta as the major mediator. *J Am Soc Nephrol Suppl* 1: S55–S57, 2004.